bioRxiv preprint doi: https://doi.org/10.1101/2023.01.18.524651; this version posted January 20, 2023. The copyright holder for this preprint (which was not certified by peer review) is the author/funder. All rights reserved. No reuse allowed without permission.

Regulation of Ebola GP conformation and membrane binding by the chemical environment of the late endosome

Aastha Jain[1], Ramesh Govindan[1,2], Alexander Berkman[1], Jeremy Luban[3,4], Natasha D. Durham[1], James B. Munro[1,4*]

[1]Department of Microbiology and Physiological Systems, UMass Chan Medical School, Worcester, MA, USA

[2]Medical Scientist Training Program, Tufts University School of Medicine, Boston, MA

[3]Program in Molecular Medicine, UMass Chan Medical School, Worcester, MA

[4]Department of Biochemistry and Molecular Biotechnology, UMass Chan Medical School, Worcester, MA

*Correspondence: james.munro@umassmed.edu

Abstract

Interaction between the Ebola virus envelope glycoprotein (GP) and the endosomal membrane is an essential step during virus entry into the cell. Acidic pH, Ca^{2+}, and removal of the glycan cap from GP have been implicated in mediating the GP-membrane interaction. However, the molecular mechanism by which these factors regulate the conformational changes that enable engagement of GP with the target membrane is unknown. Here, we apply fluorescence correlation spectroscopy (FCS) and single-molecule Förster resonance energy transfer (smFRET) to elucidate how the chemical environment of the late endosome promotes GP-membrane interaction, thereby facilitating virus entry. We first investigate the role of anionic phospholipids, phosphatidylserine (PS) and bis(monoacylglycero)phosphate (BMP), which are found in the membrane of the late endosome. We find that these lipids enable robust binding of GP to membranes in a pH- and Ca^{2+}-dependent manner. We then identify residues in GP that sense pH and trigger conformational changes that make the fusion loop available for insertion into the membrane. Molecular dynamics (MD) simulations suggest the structural basis for pH-trigger conformational changes. We similarly confirm residues in the fusion loop that mediate GP's interaction with Ca^{2+}, which likely promotes local conformational changes in the fusion loop and mediates electrostatic interactions with the anionic phospholipids. Collectively, our results provide a mechanistic understanding of how the environment of the late endosome regulates the timing and efficiency of virus entry.

bioRxiv preprint doi: https://doi.org/10.1101/2023.01.18.524651; this version posted January 20, 2023. The copyright holder for this preprint (which was not certified by peer review) is the author/funder. All rights reserved. No reuse allowed without permission.

Introduction

Ebola (EBOV) is an enveloped, negative-stranded RNA virus, which causes disease in humans with an average case fatality rate of 50% (Salata et al., 2019). Since its discovery, there have been several outbreaks of EBOV disease in sub-Saharan Africa with the most recent being in September 2022 ("Ebola returns: back to square one", 2022). Incidences of repetitive outbreaks, changes in virulence, or emergence of resistance could reduce the effectiveness of currently approved vaccination and treatment regimes. Therefore, a better understanding of the EBOV entry mechanism, an under-utilized drug target, would aid in the development of effective prophylactic and treatment interventions.

The EBOV fusion and entry process is not fully decoded. It is well known that the EBOV envelope glycoprotein (GP), present on surface of the virion, mediates virus entry in host cells. GP is a timer of heterodimers with each protomer consisting of two subunits, GP1 and GP2, which are linked by disulfide bonds (J. E. Lee et al., 2008). The virions attach to the host cell surface via GP1 interaction with C-type lectins and phosphatidylserine receptors, and are internalized by macropinocytosis (Mulherkar et al., 2011; Nanbo et al., 2010). Once inside the endosomes, cathepsins B and L proteolytically remove the mucin-like domain and glycan cap from GP1, enabling its binding to the endosomal receptor, the Niemann-Pick C1 (NPC1) cholesterol transporter (Carette et al., 2011; Chandran et al., 2005; Côté et al., 2011; Miller et al., 2012). Additional factors yet to be identified are likely required to trigger the conformational changes in GP that are necessary to promote fusion of the viral and endosomal membranes (Fénéant et al., 2019).

While in the endocytic pathway, acidification of the endosomal lumen and Ca^{2+} play critical, but poorly defined roles in promoting EBOV entry (Brecher et al., 2012; Das et al., 2020; Nathan et al., 2020; Saeed et al., 2010; Sakurai et al., 2015). In a study conducted on the isolated GP fusion loop (residues 507-560), conserved residues were mutated to identify pH sensors that trigger membrane binding (J. Lee et al., 2016). Mutation of H516 reduced lipid mixing promoted by the fusion loop by 80% in an *in vitro* assay. However, no difference in virus-like particle entry into mammalian cells could be seen with respect to wild type. This study suggested that instead of a single amino acid residue acting as a pH sensor, the effect of changes in pH is spread over multiple residues that collectively influence the conformational changes of GP. Another study investigated the interaction of Ca^{2+} ions with anionic residues flanking the fusion loop (Nathan et al., 2020). Residues D522 and E540 were especially crucial for interaction of the isolated fusion loop with Ca^{2+}, which enhances membrane binding. Our previous single-molecule Förster resonance energy transfer (smFRET) experiments on trimeric GP on the surface of pseudoviral particles demonstrated that low pH and Ca^{2+} play a critical role in promoting

bioRxiv preprint doi: https://doi.org/10.1101/2023.01.18.524651; this version posted January 20, 2023. The copyright holder for this preprint (which was not certified by peer review) is the author/funder. All rights reserved. No reuse allowed without permission.

conformational changes in GP that correlate with lipid mixing (Das et al., 2020). While prior studies had suggested residues in the fusion loop that are involved in sensing pH and Ca^{2+}, the role of these residues in mediating conformational changes of trimeric GP was not evaluated. Nor has it been determined how additional residues outside of the fusion loop might allosterically regulate conformational dynamics of GP and fusion loop-mediated membrane binding.

Lipids in host cell membranes can facilitate virus attachment and regulate fusion. Lipid content of endosomes is important in sorting of enveloped viruses into specific compartments and avoiding premature fusion (Mazzon & Mercer, 2014). The late endosomal membrane is rich in anionic lipids, phosphatidylserine (PS) and bis(monoacylglycero)phosphate (BMP) (Hullin-Matsuda et al., 2014; Urade et al., 1988). BMP is essential for fusion of viruses such as Dengue, Lassa, Uukuniemei and vesicular stomatitis virus that enter cells through the endocytic route (Bitto et al., 2016; Markosyan et al., 2021; Matos et al., 2013; Nour et al., 2013; Zaitseva et al., 2010). However, a role for BMP in EBOV GP entry could not be verified using a cell-cell fusion assay (Fénéant et al., 2019). This may indicate that the plasma membrane lacks other lipid or protein components, which are specific to the endosome and essential for EBOV GP-mediated fusion. Therefore, whether endosomal lipids play a role in EBOV entry remains an open question.

In the present study, we sought to elucidate the mechanistic basis for how the chemical features of the late endosome enable GP to engage the target membrane prior to fusion. To probe the ability of trimeric GP to bind membranes of distinct composition, we developed a fluorescence correlation spectroscopy (FCS) assay. FCS provides quantitative information on the diffusion of molecules in solution. In comparison to conventional pull-down or membrane flotation methods, FCS has high spatio-temporal resolution, requires low sample quantity, and provides rapid experimental throughput (Betaneli et al., 2019). Our results indicate that anionic lipids PS and BMP, enhanced the extent of membrane binding of GP at acidic pH and in presence of Ca^{2+}. smFRET imaging indicated that acidic pH and Ca^{2+} destabilized the pre-fusion conformation, allowing the fusion loop to move away from its hydrophobic cleft to a position where it can engage the membrane. The presence of the target membrane captured the fusion loop in a position distal to the base of the GP trimer. The results of mutagenesis support a model in which pH- and Ca^{2+}-sensing residues tune the responsiveness of GP to the chemical environment of the late endosome, ensuring proper timing of conformational changes necessary for fusion.

Results

Anionic lipids and Ca^{2+} mediate GP-membrane binding at acidic pH

bioRxiv preprint doi: https://doi.org/10.1101/2023.01.18.524651; this version posted January 20, 2023. The copyright holder for this preprint (which was not certified by peer review) is the author/funder. All rights reserved. No reuse allowed without permission.

We first sought to test the hypothesis that coordination of Ca^{2+} in the fusion loop of GP might aid in engagement of GP with anionic phospholipids found in the late endosome. To this end, we developed an FCS assay to monitor GP-membrane interactions. We prepared liposomes to mimic the endosomal membrane using phosphatidylcholine (PC), PS, BMP, and cholesterol (Ch). The trimeric ectodomain of GP (GPΔTM) from the Mayinga strain of EBOV, lacking the transmembrane domain and the mucin-like domain was expressed and purified in Expi293 cells. A foldon trimerization domain was introduced at the C-terminus to preserve the trimeric form of GPΔTM. GP1 and GP2 in GPΔTM were site-specifically labelled with Cy5 using an enzymatic labelling approach (Materials and Methods) (Durham et al., 2020). We noted that thermolysin, which is commonly used to remove the glycan cap from GP1 in place of the endosomal cathepsin proteases, led to removal of the fluorophore. To alleviate this off-target effect of thermolysin, the thermolysin cleavage site was replaced with the HRV3C protease recognition sequence. This enabled equivalent removal of the glycan cap from GP1 (forming GP^{CL}) and left the Cy5 labelling intact (**Figure S1A**). In a pseudovirion infectivity assay, introduction of the HRV3C sequence left GP 85% functional as compared to wild-type GP (**Figure S1B**).

As measured by FCS, the labelled GP^{CL} diffused as a single homogeneous species with a diffusion time of 0.308 ± 0.007 ms (**Figure 1A, B**). In contrast, 100-nm diameter liposomes diffused more slowly with a diffusion time of 2.6 ± 0.2 ms, reflecting their larger size (**Figure 1C**). To allow labelled GP^{CL} to bind liposomes under conditions that approximate the late endosome, GP^{CL} was incubated with liposomes at 37°C for 20 mins at pH 5.5 across a range of Ca^{2+} concentrations. Evaluation with FCS indicated a mixture of two species with diffusion times consistent with unbound GP^{CL}, and GP^{CL} bound to liposomes. When liposomes were composed only of PC and cholesterol (PC:Ch 95:5) only 4.8 ± 0.1% of GP^{CL} bound to liposomes in the absence of Ca^{2+} (**Figure 2**). With the addition of 1 μM Ca^{2+}, GP^{CL} binding increased to 7.9 ± 0.2%. Increasing Ca^{2+} concentration as high as 1 mM did not further promote GP^{CL} binding to the liposomes.

In contrast, when we introduced negatively charged PS into the liposomes (PC:PS:Ch 55:40:5), GP^{CL} binding increased to 10.9 ± 0.2% in the absence of Ca^{2+}. Addition of Ca^{2+} at concentrations 1 μM and 10 μM further increased GP^{CL} binding to 17.9 ± 0.3% and 27.5 ± 0.2%, respectively. However, further increases in Ca^{2+} concentration to 0.1 mM and 1 mM, reduced GP^{CL} binding by more than 1.3 and 4-fold, respectively. Next, we evaluated the effect of BMP, a negatively charged lipid unique to late endosomal membranes, on binding of GP^{CL} to liposomes (Bissig & Gruenberg, 2013; Hullin-Matsuda et al., 2014). Liposomes designed to mimic the late endosome (PC:PS:BMP:Ch 40:40:15:5) (Bissig & Gruenberg, 2013) bound 26.7 ± 0.2% of GP^{CL} in the absence of Ca^{2+}. Gradually increasing Ca^{2+} promoted GP^{CL} binding to the liposomes, reaching a peak of 52.0 ± 0.3 % bound GP^{CL} at 1 mM Ca^{2+}.

bioRxiv preprint doi: https://doi.org/10.1101/2023.01.18.524651; this version posted January 20, 2023. The copyright holder for this preprint (which was not certified by peer review) is the author/funder. All rights reserved. No reuse allowed without permission.

These data demonstrate that anionic lipids, especially BMP, promote GP^{CL}-membrane interaction in a Ca^{2+}-dependent manner.

Previous reports have shown that removal of the glycan cap and acidic pH are critical for trimeric GP to bind target membranes and promote lipid mixing in the absence of BMP (Brecher et al., 2012; Das et al., 2020). We therefore tested whether the presence of BMP affected the importance of glycan cap removal or pH during membrane binding. At neutral pH, 8 ± 1.7% GPΔTM bound to BMP-containing liposomes, with minimal increase in the presence of 1 mM Ca^{2+} (**Figure 3A**). At pH 5.5, binding increased slightly to 18.3 ± 2%, with 1 mM Ca^{2+} promoting binding further. GP^{CL} bound liposomes at neutral pH to a similarly modest extent as GPΔTM, irrespective of Ca^{2+}. Binding was increased by acidic pH and Ca^{2+} to a greater extent than that seen for GPΔmuc, reasserting the significance of glycan cap cleavage in membrane binding of GP (**Figure 3B**). Taken together, these results demonstrate that neither anionic lipids nor Ca^{2+} are sufficient to promote GP-membrane interactions at neutral pH. At acidic pH the combination of anionic lipids and Ca^{2+} facilitates robust GP^{CL} engagement with the membrane.

Mutation of histidine residues in GP^{CL} have differential effects on membrane binding

We next tested the pH sensing potential of histidine residues in GP1 and GP2. Residues H139, H154, H197, H516 and H549 were selected. Residue H139 was selected since it is present in the NPC1-binding site of GP1. Similarly, H154 is proximal to the NPC1-binding site and interacts with hydrophobic residues in the fusion loop, potentially stabilizing the pre-fusion conformation (J. E. Lee et al., 2008). H197 resides adjacent to the glycan cap cleavage site near the C-terminus of GP1. Finally, H516 and H549 flank the fusion loop and have a functional role during lipid mixing *in vitro* (J. Lee et al., 2016). H39 was not included in our analysis as its location near the N terminus of GP1 and the lack of intramolecular interactions outside of its immediate proximity make it less likely to contribute to mediating the global conformation of GP. The following pKa values for the selected histidine residues were predicted by PropKa: 5.2 (H139), 5.2 (H154), 6.9 (H516) and 7.2 (H549), suggesting that the protonation state of these residues may change under physiological conditions, which encouraged us to experimentally test these residues as putative pH sensors (Olsson et al., 2011; Søndergaard et al., 2011). The predicted pKa for H39 was 8.3, further deemphasizing this residue as a potential sensor of physiological pH change. H197 is not present in the available GP structures and thus a predicted pKa was not calculated. We next introduced alanine substitutions at positions 139, 154, 197, 516, and 549 in GP1 and GP2. The expression and structure of the mutant proteins was verified by western blot and ELISA using KZ52, an antibody specific to the native tertiary structure of GP (**Figure S2**) (J. E. Lee et al., 2008; Maruyama et al., 1999). GP-membrane interaction was evaluated using our FCS assay with

bioRxiv preprint doi: https://doi.org/10.1101/2023.01.18.524651; this version posted January 20, 2023. The copyright holder for this preprint (which was not certified by peer review) is the author/funder. All rights reserved. No reuse allowed without permission.

PC:PS:BMP:Ch liposomes since they yielded maximal binding of GP under the conditions tested. Of the five His mutants evaluated, H139A, H154A and H516A bound liposomes at approximately 10% at neutral pH, similarly to wild-type GP^{CL} (**Figure 3C-G**). However, these mutants did not show increased membrane binding at acidic pH or in the presence of Ca^{2+}. These data suggest that H139, H154, and H516 are critical to the pH-induced enhancement of GP-membrane interaction. In contrast, the H197A mutant bound liposomes similarly to wild-type across all conditions tested, indicating that H197 does not contribute to pH-induced membrane binding. H549A binding to liposomes remained similar to wild-type at neutral pH, and at acidic pH in the absence of Ca^{2+}. However, the addition of Ca^{2+} induced no additional membrane binding. This indicates that either Ca^{2+} does not bind to the H549A mutant, or Ca^{2+} binding does not induce the effect on GP structure that promotes interaction with the membrane. Furthermore, these data show that protonation of residues H197 and H549 is not necessary for pH-enhanced membrane binding.

The putative Ca^{2+}-binding site is essential for interaction with the target membrane

A previous study demonstrated that Ca^{2+} ions interact with conserved acidic residues (D522, E523, E540 and E545) flanking the fusion loop, suggesting an important role for these residues in EBOV fusion (Nathan et al., 2020). Here, we investigated whether these residues are similarly critical to membrane binding in the context of trimeric GP^{CL}. Alanine substitutions were introduced at the putative site of Ca^{2+} binding in the fusion loop. Protein expression and native conformation were evaluated as above. The D522A and E540A mutants were well expressed and maintained native antigenicity (**Figure S2**); E523A and E545A aggregated in solution and hence were not considered further. The D522A mutant bound to PC:PS:BMP:Ch liposomes to a comparable extent as wild-type GP^{CL} at neutral pH with or without Ca^{2+} (**Figure 3H**). Under acidic conditions binding was reduced (15 ± 2%) and addition of Ca^{2+} had no effect. In contrast, the membrane binding activity of E540A was similar to wild-type at acidic pH in the absence of Ca^{2+} (30 ± 3%, **Figure 3I**). However, a reduction in membrane binding (13 ± 3%) was observed in the presence of Ca^{2+}. These findings lend further support for the idea that acidic residues flanking the fusion loop play a critical role in Ca^{2+}-mediated binding of GP to the target membrane.

Conformational dynamics of wild-type GP^{CL} during membrane binding

We first sought to better characterize the conformational equilibrium of GP^{CL} through smFRET imaging at neutral pH in the absence of Ca^{2+}. We modified a previously established smFRET imaging assay that reports on conformational changes in GP2 (**Figure 4A, B**). We used pseudoparticles with GP containing the HRV3C cleavage site and a non-natural amino acid, *trans*-cyclooct-2-ene-L-lysine (TCO*) at positions 501 and 610, which enabled labelling with Cy3- and Cy5-tetrazine. Advancements in single-

bioRxiv preprint doi: https://doi.org/10.1101/2023.01.18.524651; this version posted January 20, 2023. The copyright holder for this preprint (which was not certified by peer review) is the author/funder. All rights reserved. No reuse allowed without permission.

196 molecule detection allowed us to resolve additional FRET states beyond what had previously been
197 reported (Materials and Methods). Hidden Markov modelling (HMM) of the individual smFRET traces
198 indicated the existence of 4 states (0.24 ± 0.08, 0.49 ± 0.08, 0.72 ± 0.08, and 0.92 ± 0.08) (**Figure 4C,**
199 **S4A**). The 0.92-FRET state (high FRET), which is consistent with the pre-fusion conformation reflected
200 in structures of GP (J. E. Lee et al., 2008; Zhao et al., 2016), predominated with 41 ± 1% occupancy at
201 pH 7.5 in the absence of Ca^{2+} (**Figure 4D**). HMM analysis indicated spontaneous transitions among the
202 other three FRET states and enabled construction of transition density plots (TDPs), which display the
203 relative frequency of transitions between each FRET state (**Figure 4E**). The TDP indicates that most
204 transitions occur in and out of the 0.92-FRET state, and between the 0.72- and 0.42-FRET states.
205 Transitions to and from the 0.24-FRET state were comparatively rare. Acidification to pH 5.5 reduced
206 the occupancy of the pre-fusion conformation to 21 ± 2% and resulted in more frequent transitions in
207 and out of the 0.24-FRET state (**Figure 4F**). Addition of 1 mM Ca^{2+} led to a further 2-fold reduction in
208 pre-fusion occupancy to 13±2%, and further increase in transitions to and from the 0.24-FRET state
209 (**Figure 4G**). Structures of GP in the pre-fusion conformation depict the fusion loop in a hydrophobic
210 cleft in the neighbouring protomer within the trimer (J. E. Lee et al., 2008; Zhao et al., 2016). Given
211 the sites of fluorophore attachment, we hypothesized that the low-FRET states (0.24 and 0.49 FRET)
212 might reflect conformations in which the fusion loop was released from the hydrophobic cleft to
213 positions where it can engage the target membrane. We therefore incubated the labelled
214 pseudovirions with PC:PS:BMP:Ch liposomes at pH 5.5 in the presence of 1 mM Ca^{2+}, exactly as in our
215 FCS experiments that indicated robust membrane binding. Interaction with liposomes further
216 decreased occupancy in the pre-fusion conformation to 5 ± 2% and increased the 0.24-FRET state
217 occupancy to 62 ± 1%. Overall dynamics decreased drastically with remaining transitions occurring in
218 and out of the 0.24-FRET state (**Figure 4H**). Taken together, these data identify 0.24 FRET as indicating
219 a GP^{CL} conformation that is enriched at pH 5.5 and Ca^{2+}, and further stabilized by interaction with a
220 target membrane.

221 ***Conserved histidines mediate GP^{CL} conformation at acidic pH***

222 Having identified histidine residues that are critical to GP-membrane interaction, we next sought to
223 determine the role of these residues in mediating GP conformational changes using smFRET. Similar
224 to wild-type GP^{CL}, the pre-fusion conformation (0.92 FRET) was predominant for H139A at pH 7.5 with
225 an occupancy of 37 ± 1%. However, unlike wild-type GP^{CL} the pre-fusion conformation occupancy of
226 H139A was reduced only by about 30% at acidic pH (compared to 50% for wild-type) indicating a
227 reduced sensitivity to pH (**Figure 5A**). Nonetheless, transitions to intermediate- and low-FRET states
228 increased at acidic pH to a greater extent than wild-type, which correlates with the higher infectivity
229 (**Figure S1C**). This indicates a maintained ability of H139A to undergo conformational changes (**Figure**

bioRxiv preprint doi: https://doi.org/10.1101/2023.01.18.524651; this version posted January 20, 2023. The copyright holder for this preprint (which was not certified by peer review) is the author/funder. All rights reserved. No reuse allowed without permission.

4F, 5B) but perhaps a greater dependence on NPC1 binding, which follows exposure to acidic pH in the endosome, for stabilization of functional conformations. The H154A mutant showed a more pronounced phenotype where its conformational equilibrium was insensitive to acidification, with a modest increase in transitions to low FRET (**Figure 5A, C**). While occupancy of the pre-fusion conformation remained at approximately 25% at both pH values tested, predominant occupancy was seen in the 0.49-FRET state (**Figure S4C**). Thus, while the H154A mutation destabilizes the pre-fusion conformation, the lack of sensitivity to acidic pH prevented access to a conformation competent for membrane binding. Taken together with the loss of infectivity of the H154A mutant (**Figure S1C**) (Manicassamy et al., 2005), these data support the identification of H154 as a critical sensor of acidic pH and mediator of GP conformation. Finally, consistent with H197 residing in an unstructured loop, not clearly engaged in intramolecular interactions, the H197A mutation had minimal impact on GP conformation or function as compared to wild-type at the pH tested (**Figure 5D, S1C, S4D**).

Two histidine residues in GP2, H516 and H549, had distinct effects on GP conformation. The H516A mutation induced a loss of sensitivity to changes in pH (**Figure 5A, E**), consistent with the observed dysfunction in membrane binding and lack of infectivity (**Figure S1C**). Similar to the H154A mutant, a slight increase in dynamics was seen and increased occupancy in the 0.49-FRET state (**Figure S4E**), further indicating that this conformation is not competent for membrane binding. These data support H516 also being a critical pH sensor and mediator of GP conformation. In contrast, the H549A mutant underwent significant destabilisation of the pre-fusion conformation upon exposure to acidic pH, as well as an increase in dynamics (**Figure 5A, F, S4F**). This observation correlates with the maintenance of membrane binding under acidic conditions (in the absence of Ca^{2+}) and the modest decrease in infectivity (**Figure S1C**). Thus, these data suggest that, while H549 may sense changes in pH, it is not a determinant of global GP conformation.

Modulation of GP conformation by Ca^{2+}-coordinating residues

We next asked whether the coordination of Ca^{2+} impacts GP conformation as part of its role in enabling membrane binding. The D522A mutant, which is defective in Ca^{2+} coordination, membrane binding, and infectivity, demonstrated a conformational equilibrium similar to wild-type GP at neutral pH in the absence of Ca^{2+} (**Figure 6A**) (Nathan et al., 2020). A slight increase in dynamics was observed as compared to wild-type GP, suggestive of the mutation increasing mobility of the N terminus and fusion loop (**Figure 6B**). Acidification destabilized the pre-fusion conformation, consistent with the D522A mutation not affecting sensitivity to pH (**Figure S4G**). As expected, the addition of Ca^{2+} had no effect on the stability of the pre-fusion conformation (**Figure 6A**). In contrast, the E540A mutation, which maintains functionality in membrane binding in the absence of Ca^{2+}, showed a destabilized pre-fusion

bioRxiv preprint doi: https://doi.org/10.1101/2023.01.18.524651; this version posted January 20, 2023. The copyright holder for this preprint (which was not certified by peer review) is the author/funder. All rights reserved. No reuse allowed without permission.

conformation as compared to wild-type even at neutral pH, again suggestive of increased N terminus and fusion loop mobility. Acidification had minimal effect on the conformational equilibrium, although dynamics increased slightly. In particular, transitions in and out of the low-FRET state increased as seen for wild-type GP (**Figure 6C**). The addition of Ca^{2+} led to stabilization of the 0.72-FRET state, suggesting that adopting this conformation is not sufficient for membrane binding (**Figure S4H**). Taken together, these data on the D522A and E540A mutants clarify that coordination of Ca^{2+} is not critical for destabilizing the pre-fusion conformation. Rather, the importance of Ca^{2+} coordination likely comes at a later stage during interaction with the target membrane.

Structural basis for pH-induced conformational changes

Finally, we investigated the structural basis for pH-induced conformational changes in GP^{CL} using molecular dynamics (MD) simulation. We focused our attention on H154 and H516 as our experimental data implicated these residues in sensing changes in pH. We developed atomistic models of GP^{CL} using available coordinates (Materials and Methods) (Bornholdt et al., 2016). In one model, histidine side chains were deprotonated to probe electrostatic interactions that would predominate at neutral pH. In an alternative model, histidine side chains were fully protonated to approximate the conditions of the acidic late endosome (pH 5-5.5). In both cases, the models were solvated in explicit water and charge-neutralized with ions. Following energy minimization and equilibration, we analysed the local dynamics in the proximity of H154 and H516 in a 225-ns simulation. The H154 side chain is engaged in electrostatic interactions with the side chain of E178, which contacts the receptor-binding site via interaction with R85. At the same time, the backbone carbonyl of H154 interacts electrostatically with the backbone amide N of Y534 in the fusion loop of the neighbouring protomer (**Figure 7A**). H154 thus provides a linkage between the receptor-binding site and the fusion loop, potentially stabilizing both regions in the pre-fusion conformation. According to our simulation, protonation of H154 strengthens the interaction with E178, which pulls H154 away from Y534. This movement destabilizes the H154-Y534 interaction, leading to greater relative movement of these residues (**Figure 7B**). The simulation, therefore, suggests that protonation of H154 contributes to release of the fusion loop from the hydrophobic cleft, facilitating its interaction with the target membrane. Mutation of H154 would break the linkage with E178, enabling stable contact with Y534 across a range of pHs. The simulation thus provides a rationale for our experimental observation that the GP2 conformation of the H154A mutant showed decreased sensitivity to acidic pH.

H516 flanks the fusion loop and is engaged in Pi-Pi stacking interaction with the side chain of W104 in GP1. Here again, this interaction likely mediates the stability of the fusion loop in the pre-fusion conformation. Our MD simulation suggests that this interaction is labile when H516 is deprotonated,

bioRxiv preprint doi: https://doi.org/10.1101/2023.01.18.524651; this version posted January 20, 2023. The copyright holder for this preprint (which was not certified by peer review) is the author/funder. All rights reserved. No reuse allowed without permission.

with H516 sampling multiple conformations (**Figure 7C, D**). These dynamics can be parameterized by the distance between H516 and W104, and the χ_2 dihedral angle of the H516 side chain. Protonation of H516 stabilized the stacking interaction with W104, reducing the dynamics of H516 and selecting a single pre-existing conformation (**Figure 7E**). These data imply that GP1-GP2 interaction may be critical to GP2 conformational changes that remove the fusion loop from the hydrophobic cleft. The H516-W104 interaction may aid in ensuring proper positioning of the fusion loop for initial interaction with the membrane. This would likely require that GP1 is repositioned in response to acidic pH. Mutation of H516 may serve to decouple fusion loop release from putative GP1 movement.

Discussion

Previous studies indicate critical roles for acidic pH, Ca^{2+}, removal of the glycan cap, and NPC1 binding during EBOV entry and GP-induced membrane fusion (Brecher et al., 2012; Carette et al., 2011; Côté et al., 2011; Das et al., 2020; Gregory et al., 2011; Miller et al., 2012; Nathan et al., 2020; Sakurai et al., 2015). However, live-cell imaging and cell-cell fusion experiments have demonstrated that additional factors are necessary for completion of membrane fusion (Fénéant et al., 2019; Simmons et al., 2016; Spence et al., 2016). In the present study, using a new developed FCS assay to quantify the interactions between GP and liposomes, we show that endosomal anionic lipids, including PS and BMP, promote Ca^{2+}-dependent membrane binding of GP^{CL} at acidic pH. Under the conditions tested, membrane binding was optimal in the presence of both PS and BMP. It has been shown that Ca^{2+} binds to PS in phospholipid bilayers and reduces its overall surface charge, which could explain the reduction in binding of GP^{CL} with PC:PS:Ch liposomes at Ca^{2+} concentration higher than 10 µM in our experimental setup (Martín-Molina et al., 2012; Melcrová et al., 2016). The additional presence of BMP in liposomes drastically increased GP^{CL}-membrane binding. Additionally, unlike PC:PS:Ch liposomes, increasing Ca^{2+} concentration did not limit interaction of GP^{CL} with PC:PS:BMP:Ch liposomes. Rather, an increase in GP^{CL} binding was observed with increasing Ca^{2+} concentration with maximal binding at 1 mM Ca^{2+}. Previous observations indicate that the unique structure of BMP alters the negative spontaneous curvature of membranes (Matsuo et al., 2004). Additionally, BMP increases the net surface charge of liposomes, enhancing their interaction with Ca^{2+} (Kobayashi et al., 2002). Both features of BMP may promote efficient interaction between GP^{CL} and the target membrane. In the latter case, GP^{CL} could preferentially interact with BMP via Ca^{2+} coordination within the fusion loop. Since BMP is exclusively present in the late endosome (Kobayashi et al., 2002), it could also regulate the timing of fusion of EBOV by avoiding pre-mature engagement of the fusion loop with a membrane prior to arrival in the late endosome. A similar dependence on BMP has been reported for other enveloped viruses such as Dengue virus, Lassa virus, vesicular stomatitis virus, and influenza virus (Mannsverk et al., 2022; Markosyan et al., 2021; Matos et al., 2013; Zaitseva et al., 2010).

bioRxiv preprint doi: https://doi.org/10.1101/2023.01.18.524651; this version posted January 20, 2023. The copyright holder for this preprint (which was not certified by peer review) is the author/funder. All rights reserved. No reuse allowed without permission.

Whether downstream events during EBOV fusion are also accelerated by BMP, as reported for Lassa virus, will be the topic of future studies (Markosyan et al., 2021).

The conformational changes in GP^{CL} under conditions favourable for membrane binding were elucidated by a previously validated smFRET imaging assay developed in our lab, which reports on the movement of the N-terminus of GP2 (Das et al., 2020). In the present work, we show that acidification of pH followed by addition of Ca^{2+} leads to a sequential destabilization of the pre-fusion conformation of GP^{CL}. An increase in low FRET under the same conditions suggests movement of the N terminus. This change in FRET efficiency (ΔFRET = 0.68) equates to an increase in the distance between the fluorophores of more than 30 Å. A movement of this magnitude likely also incorporates displacement of the fusion loop away from the hydrophobic cleft to a position that is competent for membrane binding. This interpretation is supported by our smFRET data acquired following incubation of GP^{CL} with liposomes at acidic pH in the presence of Ca^{2+}, which led to further destabilization of the high-FRET pre-fusion conformation, stabilization of the low-FRET conformation, and reduction of overall kinetics (**Figure 4B, C**)**.** A structural description of the low-FRET conformation will require additional FRET pairs, which report more explicitly and with more sensitivity on the position of the fusion loop. The hypothesized extended pre-hairpin intermediate in which the heptad repeat helix 1 (HR1) has linearized may require repositioning or dissociation of GP1. Here again, additional FRET pairs that report on inter-domain dynamics will be beneficial. Whatever the precise structural description of the low-FRET state, our FCS and smFRET imaging results indicate that the extent of GP-membrane binding is inversely correlated (Spearmen correlation r_S = -0.6813, p = 0.0127) with the occupancy of GP in the pre-fusion conformation (**Figure 8**).

Protonation of amino acid side chains is the driving force for inducing conformational changes in viral fusion proteins in response to acidification of pH. In particular, the role of histidine residues is well established in triggering membrane binding and fusion of influenza virus, Semiliki Forest virus, and human metapneumoviruses (Caffrey & Lavie, 2021; Harrison et al., 2013). Here, we report that residues H139, H154, H516 and H549 tune the responsiveness of EBOV GP to acidic pH through both stabilizing and destabilizing mechanisms. The membrane binding ability of H139A was reduced at acidic pH accompanied by poor destabilization of the pre-fusion conformation relative to wild type, indicating reduced ability to undergo pH-induced conformational changes in the absence of NPC1 *in vitro*. Nonetheless, H139A maintained greater infectivity than wild-type. This may be due to greater stability in the acidic endosome and given the proximity of H139 to the receptor-binding site, perhaps higher affinity for NPC1 inside cells. Mutants H154A and H516A emerged as the most important pH sensors. The membrane binding ability of both mutants was diminished at acidic pH and no difference in their FRET occupancies at neutral or acidic pH was observed. This indicates that the mutants are

bioRxiv preprint doi: https://doi.org/10.1101/2023.01.18.524651; this version posted January 20, 2023. The copyright holder for this preprint (which was not certified by peer review) is the author/funder. All rights reserved. No reuse allowed without permission.

insensitive to changes in pH and thus, functionally inactive **(Figure 5C, E).** Histidine residues can interact electrostatically with cationic amino acids such as lysine or arginine, forming His-Cat pairs, which are known to stabilize the pre-fusion conformations of several viral envelope glycoproteins (Harrison et al., 2013). These interactions are destabilized by protonation of histidines upon acidification, leading to repulsion between histidines and cationic amino acid, which contribute to triggering conformational changes necessary for viral fusion. In contrast, our MD simulation suggests that H154 and H516 are engaged in interactions not described by the His-Cat paradigm. These data indicate that protonation of H154 contributes to release of the fusion loop from its hydrophobic cleft through a stabilized interaction with E178. According to our analysis, the strengthened H154-E178 interaction destabilizes backbone electrostatics between H154 and Y534 in the fusion loop of the neighbouring protomer. Similarly, protonation of H516 stabilizes Pi-Pi stacking interaction with W104 in GP1. Thus, an inter-subunit interaction is strengthened under conditions that promote membrane binding. This interaction may mediate positioning and stability of the fusion loop and may indicate that GP1 remains associated with GP2 until after engagement with the target membrane. NPC1 binding to GP1 may partially serve to localize EBOV on the endosomal membrane to increase the efficiency with which the fusion loop inserts into the membrane. At this point, an additional endosomal factor may be required to enable transition to the post-fusion conformation, which putatively requires dissociation of GP1.

Mutagenesis of H549 did not affect membrane binding or the extent of destabilization of the pre-fusion conformation of GP at acidic pH, indicating that it is less critical for mediating changes in the global conformation of GP. Additionally, membrane binding of H549A was insensitive to the presence of Ca^{2+}. This could be due to H549A attaining a local conformation that is unresponsive to Ca^{2+}. These results suggest that H549 more likely regulates the local conformation of the fusion loop, rather than the release from the hydrophobic cleft. Taken together, our data indicate that acidic pH destabilizes the interactions within GP1, and between GP1 and GP2 by direct side-chain protonation of key histidine residues, similar to influenza HA1 and HA2 (Caffrey & Lavie, 2021; Harrison et al., 2013).

Ca^{2+} has been implicated in the fusion processes of Rubella virus, MERS-CoV, SARS-CoV-1 and -2, and EBOV (Dubé et al., 2014; Lai et al., 2017; Nathan et al., 2020; Singh et al., 2022; Straus et al., 2020). Ca^{2+} can assist in membrane fusion through coordination by anionic residues in the fusion loop, as first seen for the Rubella virus E1 glycoprotein. This may stabilize a fusion loop conformation that is optimal for insertion into the membrane. In addition, Ca^{2+} coordination in the fusion loop can affect the physical properties of the target membrane in a manner that promotes fusion (Lai et al., 2017). Previous studies have shown that compounds that lead to accumulation of Ca^{2+} in endosomes inhibit EBOV entry, which indicates that EBOV fusion is highly sensitive to endosomal Ca^{2+} concentration (Das

bioRxiv preprint doi: https://doi.org/10.1101/2023.01.18.524651; this version posted January 20, 2023. The copyright holder for this preprint (which was not certified by peer review) is the author/funder. All rights reserved. No reuse allowed without permission.

et al., 2020; Johansen et al., 2013). *In vitro* studies have demonstrated that Ca^{2+} concentrations greater than 500 µM are antagonistic to lipid mixing and fusion activity of Rubella virus, SARS-CoV-2, and EBOV (Das et al., 2020; Dubé et al., 2014; Singh et al., 2022). A previous study of the isolated fusion loop of EBOV GP highlighted the role of anionic residues, D522 and E540, in interaction with Ca^{2+} during membrane binding and lipid mixing (Nathan et al., 2020). Our findings support these conclusions and demonstrate that sensitivity of the native GP trimer to Ca^{2+}, and its ability to engage the target membrane in the presence of Ca^{2+}, is mediated by residues D522 and E540. The mutant D522A displayed destabilization of the pre-fusion conformation comparable to wild-type at acidic pH. Given the loss of membrane binding by the D522A mutant, these data indicate that acidification of pH is the major driver of global GP conformation, whereas Ca^{2+} binding may influence the local conformation of the fusion loop, enabling optimal insertion into the membrane. On the contrary, there was no significant change in the global conformation of E540A after acidification of pH. However, efficient membrane binding of E540A at acidic pH, coupled with an increase in the frequency of transitions, points toward a role for the target membrane in selecting conformations in E540A. Addition of Ca^{2+} enriched the 0.72 FRET state, reduced both conformational transitions and membrane binding of E540A. These data suggest that Ca^{2+} still binds the fusion loop of the E540A trimer in such a manner that restricts the movement necessary for membrane binding. The NMR structure of the fusion loop in DPC micelles at acidic pH shows a 90° bend, which reduces the distance between residues D522 and H549, and between E540 and E545, bringing them within ~5 Å (Gregory et al., 2011). This could reflect a conformation that becomes accessible to the fusion loop after transitioning out of the hydrophobic cleft. The insensitivity of H549A to Ca^{2+} and its proximity to D522 at acidic pH in the NMR-derived structure might suggest that this conformation is stabilized by Ca^{2+}, perhaps through coordination by these pairs of residues. Structural studies of the intact trimer, performed under conditions that promote membrane fusion, are needed to elucidate the global GP conformation and the local fusion loop configuration that enables engagement with the target membrane. Biophysical interrogations such as those presented here should guide these future studies by identifying conditions that promote functional conformations and the residues that mediate their stability.

Material and Methods

Cell lines

Expi293F cells (Gibco, ThermoFisher Scientific, Waltham, MA) were cultured in Expi293 expression medium in an orbital shaking incubator at 37°C, 8% CO_2, 125rpm. HEK293T FirB cells, which have high furin expression, were a kind gift from Dr. Theodore C. Pierson (Emerging Respiratory Virus section, Laboratory of Infectious Diseases, NIH, Bethesda, MD) (Mukherjee et al., 2014). These cells were cultured in DMEM (Gibco, ThermoFisher Scientific, Waltham, MA) with 10% cosmic calf serum

bioRxiv preprint doi: https://doi.org/10.1101/2023.01.18.524651; this version posted January 20, 2023. The copyright holder for this preprint (which was not certified by peer review) is the author/funder. All rights reserved. No reuse allowed without permission.

(Hyclone, Cytiva Life Sciences, Marlborough, MA) and 1% penicillin-streptomycin (Gibco, ThermoFisher Scientific, Waltham, MA) at 37°C, 5% CO_2.

Plasmids

pHLsec-GPΔTM and pMAM51-GPΔmuc plasmids were obtained from Dr. Kartik Chandran's lab (Einstein College of Medicine, NY). pHLsec-GPΔTM encodes EBOV (Mayinga) GP sequence (UniProt Q05320) with deleted mucin-like and transmembrane domains. A T4 fibritin foldon trimerization domain and 6X-histidine tag for Ni-NTA purification has been inserted into the C terminus. The A1 (*GDSLDMLEWSLM*) and A4 (*DSLSMLEW*) peptides were introduced at positions 32 and 501 in GP1 and GP2, respectively, for site-specific labelling of GPΔTM, as previously described (Durham et al., 2020). pMAM51-GPΔmuc encodes full-length GP with the mucin-like domain deleted and was used for all pseudovirion experiments. In both GPΔTM and GPΔmuc the thermolysin cleavage site, *VNAT* at position 203, was replaced with an HRV3C protease recognition site (*LEVLFQGP*) by site directed mutagenesis (Q5 site directed mutagenesis kit, New England Biolabs, Ipswich, MA). All amino acid substitutions were also introduced in GPΔTM and GPΔmuc via site-directed mutagenesis. pNL4.3.Luc.R-E- used in infectivity assays was obtained through the NIH AIDS Reagent program (contributed by Dr. Nathaniel Landau, New York University School of Medicine) (He et al., 1995). An amber stop codon (TAG) in the *tat* gene was modified by site-directed mutagenesis to --TAA to prevent readthrough during incorporation of TCO* for labelling of GPΔmuc. Plasmids $PyIRS^{AF}$ and eRF1 were provided by Dr. Edward Lemke (Johannes Gutenberg-University of Mainz, Germany).

Protein expression and purification

For production of GPΔTM proteins (wild-type and mutants), Expi293F cells were transfected with pHLsec-GPΔTM using polyethyleneimine (PEI MAX, Polysciences, Warrington, PA) at a mass ratio of 1:3 DNA:PEI MAX. As previously described, a 2:1 ratio of pHLsec-GPΔTM to tagged pHLsec-GPΔTM was transfected to ensure that GPΔTM trimers contained on average a single tagged protomer. The supernatants containing soluble GPΔTM proteins were harvested 5 days post-transfection. The proteins were purified using Ni-NTA agarose beads (Pierce, ThermoFisher Scientific, Waltham, MA). The protein was bound to the column in phosphate-buffered saline (PBS) containing 10mM imidazole, followed by washing with 20mM imidazole in PBS and elution in 200 mM imidazole containing PBS. Following purification, proteins were exchanged to labelling buffer (20 mM HEPES, 50 mM NaCl, pH 7.5) using VivaSpin 6 concentrator (Sartorius AG, Gottingen, Germany).

Labelling of GPΔTM

Wild-type and mutant GPΔTM proteins were labelled with 5 µM LD650 conjugated to coenzyme A (LD650-CoA; Lumidyne Technologies, New York, NY). The fluorophore was attached to the A1 and A4

bioRxiv preprint doi: https://doi.org/10.1101/2023.01.18.524651; this version posted January 20, 2023. The copyright holder for this preprint (which was not certified by peer review) is the author/funder. All rights reserved. No reuse allowed without permission.

peptides in the tagged GPΔTM through incubation with 5 µM acyl carrier protein synthase (AcpS) in the labelling buffer with 10 mM $Mg(CH_3COO)_2$ overnight at room temperature (Durham et al., 2020). The labelled proteins were subjected to overnight cleavage by exogenous furin (New England Biolabs, Ipswich, MA) at 37°C to fully convert GP0 to GP1 and GP2. The processed proteins were purified by size-exclusion chromatography on a Superdex 200 Increase 10/300 GL column (GE Healthcare, Chicago, IL). Purified, labelled proteins were concentrated using Amicon Ultra 30K filters (MilliporeSigma, Burlington, MA), aliquoted and stored at -80°C until further use. The concentration of proteins was determined using Bradford reagent.

Indirect ELISA

Labelled proteins were diluted to a final concentration of 5 µg/ml in PBS and coated onto the wells of a 96-well polystyrene plate (Pierce™, ThermoFisher Scientific, Waltham, MA) by incubating overnight at 4°C. The plate was washed three times with PBST (PBS with 0.1% Tween-20) followed by blocking with 5% skim milk in PBST for 3h at room temperature. The blocking solution was removed, and the plate was again washed twice with PBST. Proteins were probed with KZ52 antibody (Durham et al., 2020; Maruyama et al., 1999) at a dilution of 1:1000 overnight at 4°C. The plate was then washed and incubated with horseradish peroxidase-conjugated anti-human IgG (Invitrogen™, ThermoFisher Scientific, Waltham, MA) at a dilution of 1:2000 for 2h at room temperature. After washing the plate four times with PBST, TMB solution (3,3',5,5'-tetramethylbenzidine; ThermoFisher Scientific, Waltham, MA) was added to each well, incubated for 15 min, followed by addition of an equal volume of 2M sulphuric acid. The optical density was immediately read at 450 nm in a Synergy H1 microplate reader (BioTek, Winooski, VT).

Liposome preparation

The following lipids were used for liposome preparation: POPC (1-palmitoyl-2-oleoyl-glycero-3-phosphocholine), POPS (1-palmitoyl-2-oleoyl-sn-glycero-3-phospho-L-serine (sodium salt)), BMP (bis(monooleoylglycero)phosphate (S,R Isomer)) and cholesterol (all from Avanti Polar lipids, Alabaster, AL). Stock solution of lipids (10 mg/ml) were diluted at desired ratios in chloroform to obtain a final total lipid concentration of 1 mM. A lipid film was formed in a glass vial by evaporating the chloroform under a steady stream of Argon gas. Residual chloroform was removed by incubating the lipid film overnight under vacuum. Lipids were rehydrated with 5 mM HEPES, 10 mM MES and 150 mM NaCl, pH 7.5, for 1 hour at room temperature. The lipid suspension was vortexed 5-7 times in 10 sec pulses followed by 10 freeze-thaw cycles with liquid nitrogen. Liposomes were formed by extruding the lipid solution 37 times through a 100 nm polycarbonate membrane (Whatman® Nucleopore™ track-etched membrane) in a mini-extruder (Avanti Polar Lipids, Alabaster, AL). The size

bioRxiv preprint doi: https://doi.org/10.1101/2023.01.18.524651; this version posted January 20, 2023. The copyright holder for this preprint (which was not certified by peer review) is the author/funder. All rights reserved. No reuse allowed without permission.

of liposomes was verified using dynamic light scattering (Zetasizer Nano, Malvern Panalytical, Malvern, UK). The liposomes were stored at 4°C and used within a week.

HRV3C cleavage

The glycan cap was removed from GPΔTM and pseudovirions with GPΔmuc through incubation with HRV3C protease (Pierce™, ThermoFisher Scientific, Waltham, MA) at 10°C for 16 hr. Cleavage of LD650-labelled GPΔTM was verified by in-gel fluorescence imaging of uncleaved and cleaved protein on a 4-20% polyacrylamide using a ChemiDoc™ MP imaging system (Bio-Rad, Hercules, CA) followed by Coomassie staining.

Fluorescence correlation spectroscopy

For membrane binding studies, liposomes (500 µM total lipid) were incubated with 5 nM labelled GPΔTM in 5 mM HEPES, 10 mM MES, 150 mM NaCl (pH 7.5 or 5.5). For experiments performed in the absence of Ca^{2+}, 1mM EDTA was included to chelate any Ca^{2+} already bound to GPΔTM. Otherwise, the indicated concentration of $CaCl_2$ (0-1mM) was included in the incubation. The liposome-GPΔTM mixture was incubated at 37°C for 20 min to allow binding. For experiments performed at pH 5.5, the liposome mixture was acidified with 1 M HCl prior to addition of GPΔTM. FCS experiments were performed by dropping 50 µL of the liposome-GPΔTM mixture onto a coverslip (No. 1.5 Thorlabs, Newton, NJ). To prevent sticking of the protein-membrane complex to the glass surface, coverslips were plasma-cleaned followed by coating with 10% polyethylene glycol (PEG-8000, Promega, Madison, WI). 100 autocorrelation curves, 5 sec each in length, were recorded at room temperature using a 638 nm laser in a CorTector SX100 (LightEdge Technologies Ltd., Zhongshan City, China). The curves were fitted to the following model for two species diffusing in three dimensions with triplet blinking (Betaneli et al., 2019; Ducas & Rhoades, 2012; Rhoades et al., 2006):

$G(\tau) = G_{triplet}(\tau).\, G_{complex}(\tau)$, where

$G_{triplet}(\tau) = 1 - T + T \cdot e^{\frac{\tau}{\tau_{triplet}}}$, and

$$G_{complex}(\tau) = \frac{1}{N}\left(f \cdot \left[1 + \frac{\tau}{\tau_{protein}}\right]^{-1} \left[1 + \frac{\tau}{s^2\tau_{protein}}\right]^{-1/2} + \alpha \cdot (1 - f) \cdot \left[1 + \frac{\tau}{\tau_{liposome}}\right]^{-1} \left[1 + \frac{\tau}{s^2\tau_{liposome}}\right]^{-1/2} \right)$$

where, N is the number of molecules in the confocal volume, f is the fraction of free protein, α is the average brightness of the protein-liposome complex, $\tau_{protein}$ is the diffusion time of free protein, $\tau_{liposome}$ is the diffusion time of the liposome, and s is the structural parameter, which reflects the

bioRxiv preprint doi: https://doi.org/10.1101/2023.01.18.524651; this version posted January 20, 2023. The copyright holder for this preprint (which was not certified by peer review) is the author/funder. All rights reserved. No reuse allowed without permission.

dimensions of the confocal volume. The diffusion times, $\tau_{protein}$ and $\tau_{liposome}$ were calculated by fitting the autocorrelation curves of GPΔTM and liposomes (labelled with DiD) separately to single species diffusion models. The values of s and $\tau_{protein}$ were kept constant to calculate the fraction of free and bound protein for all samples. Due to polydispersity of liposomes and fast photophysical dynamics of triplet blinking, $\tau_{liposome}$ and $\tau_{triplet}$ were allowed to vary during fitting. The analysis was carried out in MATLAB (MathWorks, Natick, MA) using a non-linear least-square curve fitting algorithm. All values were averaged over three independent experiments.

Western blotting

All proteins and pseudovirions were run on 4-20% denaturing polyacrylamide gels (Bio-Rad, Hercules, CA) and transferred to nitrocellulose membrane using Trans-blot Turbo (Bio-Rad, Hercules, CA). Membranes were rinsed with PBST, blocked with 5% skim milk in PBST for 1 h followed by probing of GP and p24 with monoclonal antibody (mAb) H3C8 at a dilution of 1:1000, (Ou et al., 2010) and mouse mAB B1217M at a dilution of 1:2000 (Genetex, Irvine, CA), respectively. The mAb H3C8 was humanized by cloning its variable heavy and light chain fragments in human IgG expression vectors obtained from Dr. Michel Nussenzweig (The Rockefeller University). Membranes were washed three times with PBST, incubated with horseradish peroxidase-conjugated anti-human IgG (Invitrogen™, ThermoFisher, Waltham, MA) and anti-mouse IgG (ThermoFisher, Waltham, MA) for 1 h at room temperature and developed with SuperSignal™ West Pico PLUS chemiluminescent substrate (ThermoFisher Scientific, Waltham, MA).

Infectivity assay

Infectivity of VSV pseudovirions containing wild-type GPΔmuc was compared to pseudovirions containing GPΔmuc^{HRV3C} via flow cytometry (Whitt, 2010). HEK293T cells were transfected with GPΔmuc and GPΔmuc^{HRV3C} plasmid using polyethyleneimine (PEI MAX, Polysciences, Warrington, PA) at a mass ratio of 1:3 PEI MAX:DNA. Cells were transduced with VSVΔG-GFP-VSVG pseudovirions 24 h after transfection. Supernatants containing VSVΔG-GFP-GPΔmuc and VSVΔG-GFP-GPΔmuc^{HRV3C} were collected 24 h post-transduction and filtered through 0.45 µm filter. As a negative control, bald particles were generated by transducing cells not expressing GPΔmuc. Vero cells were infected with VSV pseudovirions through incubation at 37°C for 1 h with gentle agitation every 15min to allow even spread of pseudovirions. Fresh media was added, and infection was allowed to proceed for five more hours. Cells were trypsinized and assayed for expression of GFP using a flow cytometer (MACSQuant Analyzer 1.0). The results were averaged across technical replicates and standard error was calculated from biological replicates.

bioRxiv preprint doi: https://doi.org/10.1101/2023.01.18.524651; this version posted January 20, 2023. The copyright holder for this preprint (which was not certified by peer review) is the author/funder. All rights reserved. No reuse allowed without permission.

To assess infectivity of GPΔmuc^{HRV3C} mutants, pseudovirions with luciferase-expressing HIV-1 core were produced. Plasmids pMAM51-GPΔmuc^{HRV3C} and pNL4.3.Luc.R-E- were co-transfected at a ratio of 1:5 in HEK 293T FirB cells. Pseudovirions were harvested 24 h post-transfection by collecting the supernatant, passing through a 0.45 µm filter, and layering on 10% sucrose in PBS solution followed by ultracentrifugation at 25000 rpm for 2 h at 4°C. After resuspension of the pellet in PBS, particles were analyzed by western blot. The virions were cleaved with HRV3C to remove the glycan cap as above, incubated with Vero cells for 5 h at 37°C, followed by replacement of growth media. After 48 h, cells were lysed with Glo Lysis Buffer (Promega, Madison, WI) for 5 min at room temperature. Luciferase activity was recorded by mixing equal volumes of cell lysate and Steady Glo Reagent (Promega, Madison, WI) and reading in a Synergy H1 plate reader (Biotek, Winooski, VT). The luminescence was normalized to expression of GP for each sample. Bald pseudovirions containing only pNL4.3.Luc.R-E- were used as a negative control.

Pseudovirion production and labelling for smFRET imaging

To facilitate attachment of fluorophores to GP on the surface of pseudovirions for smFRET imaging, the non-natural amino acid TCO* (SiChem GmbH, Bremen, Germany) was introduced at positions 501 and 610 through amber stop codon suppression (GP*) (**Figure 4B**) (Nikić et al., 2016). Pseudovirions were produced by transfecting HEK293T FirB cells with pMAM51-GPΔmuc^{HRV3C} plasmids with and without amber stop codons at a 1:1 ratio, which equated to an excess of GP protein over GP*. This ratio was optimized to ensure that the pseudovirions rarely contained more than a single GP* protomer per particle. A plasmid encoding HIV-1 GagPol was also transfected to provide the pseudovirion core. To increase the efficiency of amber codon readthrough, plasmids eRF1 and PyIRS^{AF} were also included in transfection (Das et al., 2020; Nikić et al., 2016). The supernatant containing pseudovirions was harvested 48 h post-transfection, filtered through a 0.45 µm mixed cellulose ester membrane and layered onto 10% sucrose (in PBS) solution. The pseudovirions were pelleted by ultracentrifugation at 25000 rpm for 2 h at 4°C. Pseudovirions were resuspended in 500 µL PBS and incubated with 500 nM Cy3- and Cy5-tetrazine (Jena Biosciences, Jena, Germany) for 30 min at room temperature. 60 µM DSPE-PEG2000 biotin (Avanti Polar Lipids, Alabaster, AL) was added to the labelling reaction and incubated for another 30 min at room temperature with gentle mixing. The labelling reaction was layered on a 6-30% OptiPrep (Sigma-Aldrich, MilliporeSigma, Burlington, MA) density gradient and ultracentrifuged at 35000 rpm for 1 h at 4°C. Labelled pseudovirions were collected, aliquoted, and analyzed by western blot.

smFRET imaging assay and data analysis

bioRxiv preprint doi: https://doi.org/10.1101/2023.01.18.524651; this version posted January 20, 2023. The copyright holder for this preprint (which was not certified by peer review) is the author/funder. All rights reserved. No reuse allowed without permission.

All smFRET experiments were performed following removal of the glycan cap from GP. Labelled and glycan cap-cleaved pseudovirions were immobilized on streptavidin-coated quartz slides and imaged on a wide-field prism-based TIRF microscope (Blakemore et al., 2021). Imaging was performed in the same buffer used for the membrane binding assay (5 mM HEPES, 10 mM MES, 150 mM NaCl [pH 7.5 or 5.5]). To study the effect of Ca^{2+}, the buffer was supplemented with 1 mM $CaCl_2$. smFRET data was acquired at room temperature at 25 frames/sec using the MicroManager microscope control software (micromanager.org). Analysis of smFRET data was performed using the SPARTAN software package (https://www.scottblanchardlab.com/software) (Juette et al., 2016) in MATLAB (MathWorks, Natick, MA). smFRET trajectories were selected according to the following criteria: acceptor fluorescence intensity greater than 35; FRET was detectable for at least 15 frames prior to photobleaching; correlation coefficient between donor and acceptor fluorescence traces was less than -0.4; signal-to-noise ratio was greater than 10; and background fluorescence was less than 50. Trajectories that met these criteria were further verified manually and fitted to a 5-state linear hidden Markov model (including a zero-FRET state) using maximum point likelihood (MPL) algorithm implemented in SPARTAN (Qin et al., 2000). The 5-state linear model was chosen based on the Akaike Information Criterium (AIC) and the Bayesian Inference Criterium (BIC) (**Figure S3**) (Akaike, 1974; Schwarz, 1978). Several models were initially considered with varying numbers of model parameters and topology. The 5-state linear model minimized both the AIC and BIC criteria relative to the models considered and was thus chosen for analysis. The idealizations from total number of traces for each sample were used to calculate the occupancies in different FRET states and construct the FRET histograms and transition density plots (TDPs).

MD simulation

A model of trimeric GP^{CL} was generated from atomic coordinates determined through x-ray crystallography (PDB accession: 5JQ3) (Zhao et al., 2016). Models included residues 32-188 of GP1 and 502-598 of GP2. Missing atoms, including hydrogens were added using pdb4amber. The protein components of the models were parameterized with the Amber forcefield (ff14SB). The systems were charge neutralized and solvated with the TIP3P explicit solvent model in LEaP. The solvated proteins were energy minimized for 0.1 ns, followed by equilibration using a stepwise protocol (Shi et al., 2008). Briefly, the protein backbone was harmonically constrained, with the constraints being released stepwise over 4 0.3-ns intervals. The simulations were then run for 225 ns in the NPT ensemble. Temperature and pressure were maintained using the Langevin thermostat and the Nose-Hoover Langevin barostat, respectively. Electrostatics were calculated using the Particle Mesh Ewald algorithm. All simulation steps were run using NAMD version 2.14 on the c3ddb cluster at the Massachusetts Green High Performance Computing Center.

bioRxiv preprint doi: https://doi.org/10.1101/2023.01.18.524651; this version posted January 20, 2023. The copyright holder for this preprint (which was not certified by peer review) is the author/funder. All rights reserved. No reuse allowed without permission.

Acknowledgments

The authors would like to thank Dr. Marco Díaz-Salinas (UMass Chan Medical School, Worcester, MA) for creating substitution mutations in *tat* in pNL4.3.Luc.R-E- plasmid used in the present study. We would also like to thank Dr. Gang Han (UMass Chan Medical School, Worcester, MA) for providing the facility of dynamic light scattering. This work was supported by NIH grants R01AI174645 and R01GM143773 to J.B.M, and R01AI148784 to J.L.

References

Akaike, H. (1974). A new look at the statistical model identification. *IEEE Transactions on Automatic Control*, *19*(6), 716–723. https://doi.org/10.1109/tac.1974.1100705

Betaneli, V., Mücksch, J. & Schwille, P. (2019). Lipid-Protein Interactions, Methods and Protocols. *Methods in Molecular Biology*, *2003*, 415–447. https://doi.org/10.1007/978-1-4939-9512-7_18

Bissig, C. & Gruenberg, J. (2013). Lipid Sorting and Multivesicular Endosome Biogenesis. *Cold Spring Harbor Perspectives in Biology*, *5*(10), a016816. https://doi.org/10.1101/cshperspect.a016816

Bitto, D., Halldorsson, S., Caputo, A. & Huiskonen, J. T. (2016). Low pH and Anionic Lipid-dependent Fusion of Uukuniemi Phlebovirus to Liposomes*. *Journal of Biological Chemistry*, *291*(12), 6412–6422. https://doi.org/10.1074/jbc.m115.691113

Blakemore, R. J., Burnett, C., Swanson, C., Kharytonchyk, S., Telesnitsky, A. & Munro, J. B. (2021). Stability and conformation of the dimeric HIV-1 genomic RNA 5'UTR. *Biophysical Journal*, *120*(21), 4874–4890. https://doi.org/10.1016/j.bpj.2021.09.017

Bornholdt, Z. A., Ndungo, E., Fusco, M. L., Bale, S., Flyak, A. I., Crowe, J. E., Chandran, K. & Saphire, E. O. (2016). Host-Primed Ebola Virus GP Exposes a Hydrophobic NPC1 Receptor-Binding Pocket, Revealing a Target for Broadly Neutralizing Antibodies. *MBio*, *7*(1), e02154-15. https://doi.org/10.1128/mbio.02154-15

Brecher, M., Schornberg, K. L., Delos, S. E., Fusco, M. L., Saphire, E. O. & White, J. M. (2012). Cathepsin Cleavage Potentiates the Ebola Virus Glycoprotein To Undergo a Subsequent Fusion-Relevant Conformational Change. *Journal of Virology*, *86*(1), 364–372. https://doi.org/10.1128/jvi.05708-11

Caffrey, M. & Lavie, A. (2021). pH-Dependent Mechanisms of Influenza Infection Mediated by Hemagglutinin. *Frontiers in Molecular Biosciences*, *8*, 777095. https://doi.org/10.3389/fmolb.2021.777095

Carette, J. E., Raaben, M., Wong, A. C., Herbert, A. S., Obernosterer, G., Mulherkar, N., Kuehne, A. I., Kranzusch, P. J., Griffin, A. M., Ruthel, G., Cin, P. D., Dye, J. M., Whelan, S. P., Chandran, K. & Brummelkamp, T. R. (2011). Ebola virus entry requires the cholesterol transporter Niemann-Pick C1. *Nature*, *477*(7364), 340–343. https://doi.org/10.1038/nature10348

Chandran, K., Sullivan, N. J., Felbor, U., Whelan, S. P. & Cunningham, J. M. (2005). Endosomal Proteolysis of the Ebola Virus Glycoprotein Is Necessary for Infection. *Science*, *308*(5728), 1643–1645. https://doi.org/10.1126/science.1110656

bioRxiv preprint doi: https://doi.org/10.1101/2023.01.18.524651; this version posted January 20, 2023. The copyright holder for this preprint (which was not certified by peer review) is the author/funder. All rights reserved. No reuse allowed without permission.

663 Côté, M., Misasi, J., Ren, T., Bruchez, A., Lee, K., Filone, C. M., Hensley, L., Li, Q., Ory, D., Chandran, K.
664 & Cunningham, J. (2011). Small molecule inhibitors reveal Niemann–Pick C1 is essential for Ebola
665 virus infection. *Nature*, *477*(7364), 344–348. https://doi.org/10.1038/nature10380

666 Das, D. K., Bulow, U., Diehl, W. E., Durham, N. D., Senjobe, F., Chandran, K., Luban, J. & Munro, J. B.
667 (2020). Conformational changes in the Ebola virus membrane fusion machine induced by pH,
668 Ca2+, and receptor binding. *PLoS Biology*, *18*(2), e3000626.
669 https://doi.org/10.1371/journal.pbio.3000626

670 Diseases, T. L. I. (2022). Ebola returns: back to square one. *The Lancet Infectious Diseases*.
671 https://doi.org/10.1016/s1473-3099(22)00678-8

672 Dubé, M., Rey, F. A. & Kielian, M. (2014). Rubella Virus: First Calcium-Requiring Viral Fusion Protein.
673 *PLoS Pathogens*, *10*(12), e1004530. https://doi.org/10.1371/journal.ppat.1004530

674 Ducas, V. C. & Rhoades, E. (2012). Quantifying Interactions of β-Synuclein and γ-Synuclein with
675 Model Membranes. *Journal of Molecular Biology*, *423*(4), 528–539.
676 https://doi.org/10.1016/j.jmb.2012.08.008

677 Durham, N. D., Howard, A. R., Govindan, R., Senjobe, F., Fels, J. M., Diehl, W. E., Luban, J., Chandran,
678 K. & Munro, J. B. (2020). Real-Time Analysis of Individual Ebola Virus Glycoproteins Reveals Pre-
679 Fusion, Entry-Relevant Conformational Dynamics. *Viruses*, *12*(1), 103.
680 https://doi.org/10.3390/v12010103

681 Fénéant, L., Wijs, K. M. S., Nelson, E. A. & White, J. M. (2019). An exploration of conditions proposed
682 to trigger the Ebola virus glycoprotein for fusion. *PLoS ONE*, *14*(7), e0219312.
683 https://doi.org/10.1371/journal.pone.0219312

684 Gregory, S. M., Harada, E., Liang, B., Delos, S. E., White, J. M. & Tamm, L. K. (2011). Structure and
685 function of the complete internal fusion loop from Ebolavirus glycoprotein 2. *Proceedings of the*
686 *National Academy of Sciences*, *108*(27), 11211–11216. https://doi.org/10.1073/pnas.1104760108

687 Harrison, J. S., Higgins, C. D., O'Meara, M. J., Koellhoffer, J. F., Kuhlman, B. A. & Lai, J. R. (2013). Role
688 of Electrostatic Repulsion in Controlling pH-Dependent Conformational Changes of Viral Fusion
689 Proteins. *Structure*, *21*(7), 1085–1096. https://doi.org/10.1016/j.str.2013.05.009

690 He, J., Choe, S., Walker, R., Marzio, P. D., Morgan, D. O. & Landau, N. R. (1995). Human
691 immunodeficiency virus type 1 viral protein R (Vpr) arrests cells in the G2 phase of the cell cycle
692 by inhibiting p34cdc2 activity. *Journal of Virology*, *69*(11), 6705–6711.
693 https://doi.org/10.1128/jvi.69.11.6705-6711.1995

694 Hullin-Matsuda, F., Taguchi, T., Greimel, P. & Kobayashi, T. (2014). Lipid compartmentalization in the
695 endosome system. *Seminars in Cell & Developmental Biology*, *31*, 48–56.
696 https://doi.org/10.1016/j.semcdb.2014.04.010

697 Johansen, L. M., Brannan, J. M., Delos, S. E., Shoemaker, C. J., Stossel, A., Lear, C., Hoffstrom, B. G.,
698 DeWald, L. E., Schornberg, K. L., Scully, C., Lehár, J., Hensley, L. E., White, J. M. & Olinger, G. G.
699 (2013). FDA-Approved Selective Estrogen Receptor Modulators Inhibit Ebola Virus Infection.
700 *Science Translational Medicine*, *5*(190), 190ra79. https://doi.org/10.1126/scitranslmed.3005471

bioRxiv preprint doi: https://doi.org/10.1101/2023.01.18.524651; this version posted January 20, 2023. The copyright holder for this preprint (which was not certified by peer review) is the author/funder. All rights reserved. No reuse allowed without permission.

Juette, M. F., Terry, D. S., Wasserman, M. R., Altman, R. B., Zhou, Z., Zhao, H. & Blanchard, S. C. (2016). Single-molecule imaging of non-equilibrium molecular ensembles on the millisecond timescale. *Nature Methods*, *13*(4), 341–344. https://doi.org/10.1038/nmeth.3769

Kobayashi, T., Beuchat, M.-H., Chevallier, J., Makino, A., Mayran, N., Escola, J.-M., Lebrand, C., Cosson, P., Kobayashi, T. & Gruenberg, J. (2002). Separation and Characterization of Late Endosomal Membrane Domains*. *Journal of Biological Chemistry*, *277*(35), 32157–32164. https://doi.org/10.1074/jbc.m202838200

Lai, A. L., Millet, J. K., Daniel, S., Freed, J. H. & Whittaker, G. R. (2017). The SARS-CoV Fusion Peptide Forms an Extended Bipartite Fusion Platform that Perturbs Membrane Order in a Calcium-Dependent Manner. *Journal of Molecular Biology*, *429*(24), 3875–3892. https://doi.org/10.1016/j.jmb.2017.10.017

Lee, J. E., Fusco, M. L., Hessell, A. J., Oswald, W. B., Burton, D. R. & Saphire, E. O. (2008). Structure of the Ebola virus glycoprotein bound to an antibody from a human survivor. *Nature*, *454*(7201), 177–182. https://doi.org/10.1038/nature07082

Lee, J., Gregory, S. M., Nelson, E. A., White, J. M. & Tamm, L. K. (2016). The Roles of Histidines and Charged Residues as Potential Triggers of a Conformational Change in the Fusion Loop of Ebola Virus Glycoprotein. *PLoS ONE*, *11*(3), e0152527. https://doi.org/10.1371/journal.pone.0152527

Manicassamy, B., Wang, J., Jiang, H. & Rong, L. (2005). Comprehensive Analysis of Ebola Virus GP1 in Viral Entry. *Journal of Virology*, *79*(8), 4793–4805. https://doi.org/10.1128/jvi.79.8.4793-4805.2005

Mannsverk, S., Giraldo, A. M. V. & Kasson, P. M. (2022). Influenza Virus Membrane Fusion Is Promoted by the Endosome-Resident Phospholipid Bis(monoacylglycero)phosphate. *The Journal of Physical Chemistry. B*, *126*(49), 10445–10451. https://doi.org/10.1021/acs.jpcb.2c06642

Markosyan, R. M., Marin, M., Zhang, Y., Cohen, F. S. & Melikyan, G. B. (2021). The late endosome-resident lipid bis(monoacylglycero)phosphate is a cofactor for Lassa virus fusion. *PLoS Pathogens*, *17*(9), e1009488. https://doi.org/10.1371/journal.ppat.1009488

Martín-Molina, A., Rodríguez-Beas, C. & Faraudo, J. (2012). Effect of calcium and magnesium on phosphatidylserine membranes: experiments and all-atomic simulations. *Biophysical Journal*, *102*(9), 2095–2103. https://doi.org/10.1016/j.bpj.2012.03.009

Maruyama, T., Rodriguez, L. L., Jahrling, P. B., Sanchez, A., Khan, A. S., Nichol, S. T., Peters, C. J., Parren, P. W. H. I. & Burton, D. R. (1999). Ebola Virus Can Be Effectively Neutralized by Antibody Produced in Natural Human Infection. *Journal of Virology*, *73*(7), 6024–6030. https://doi.org/10.1128/jvi.73.7.6024-6030.1999

Matos, P. M., Marin, M., Ahn, B., Lam, W., Santos, N. C. & Melikyan, G. B. (2013). Anionic lipids are required for vesicular stomatitis virus G protein-mediated single particle fusion with supported lipid bilayers. *The Journal of Biological Chemistry*, *288*(18), 12416–12425. https://doi.org/10.1074/jbc.m113.462028

Matsuo, H., Chevallier, J., Mayran, N., Blanc, I. L., Ferguson, C., Fauré, J., Blanc, N. S., Matile, S., Dubochet, J., Sadoul, R., Parton, R. G., Vilbois, F. & Gruenberg, J. (2004). Role of LBPA and Alix in

bioRxiv preprint doi: https://doi.org/10.1101/2023.01.18.524651; this version posted January 20, 2023. The copyright holder for this preprint (which was not certified by peer review) is the author/funder. All rights reserved. No reuse allowed without permission.

Multivesicular Liposome Formation and Endosome Organization. *Science*, *303*(5657), 531–534. https://doi.org/10.1126/science.1092425

Mazzon, M. & Mercer, J. (2014). Lipid interactions during virus entry and infection. *Cellular Microbiology*, *16*(10), 1493–1502. https://doi.org/10.1111/cmi.12340

Melcrová, A., Pokorna, S., Pullanchery, S., Kohagen, M., Jurkiewicz, P., Hof, M., Jungwirth, P., Cremer, P. S. & Cwiklik, L. (2016). The complex nature of calcium cation interactions with phospholipid bilayers. *Scientific Reports*, *6*(1), 38035. https://doi.org/10.1038/srep38035

Miller, E. H., Obernosterer, G., Raaben, M., Herbert, A. S., Deffieu, M. S., Krishnan, A., Ndungo, E., Sandesara, R. G., Carette, J. E., Kuehne, A. I., Ruthel, G., Pfeffer, S. R., Dye, J. M., Whelan, S. P., Brummelkamp, T. R. & Chandran, K. (2012). Ebola virus entry requires the host-programmed recognition of an intracellular receptor. *The EMBO Journal*, *31*(8), 1947–1960. https://doi.org/10.1038/emboj.2012.53

Mukherjee, S., Dowd, K. A., Manhart, C. J., Ledgerwood, J. E., Durbin, A. P., Whitehead, S. S. & Pierson, T. C. (2014). Mechanism and significance of cell type-dependent neutralization of flaviviruses. *Journal of Virology*, *88*(13), 7210–7220. https://doi.org/10.1128/jvi.03690-13

Mulherkar, N., Raaben, M., Torre, J. C. de la, Whelan, S. P. & Chandran, K. (2011). The Ebola virus glycoprotein mediates entry via a non-classical dynamin-dependent macropinocytic pathway. *Virology*, *419*(2), 72–83. https://doi.org/10.1016/j.virol.2011.08.009

Nanbo, A., Imai, M., Watanabe, S., Noda, T., Takahashi, K., Neumann, G., Halfmann, P. & Kawaoka, Y. (2010). Ebolavirus Is Internalized into Host Cells via Macropinocytosis in a Viral Glycoprotein-Dependent Manner. *PLoS Pathogens*, *6*(9), e1001121. https://doi.org/10.1371/journal.ppat.1001121

Nathan, L., Lai, A. L., Millet, J. K., Straus, M. R., Freed, J. H., Whittaker, G. R. & Daniel, S. (2020). Calcium Ions Directly Interact with the Ebola Virus Fusion Peptide To Promote Structure–Function Changes That Enhance Infection. *ACS Infectious Diseases*, *6*(2), 250–260. https://doi.org/10.1021/acsinfecdis.9b00296

Nikić, I., Girona, G. E., Kang, J. H., Paci, G., Mikhaleva, S., Koehler, C., Shymanska, N. V., Santos, C. V., Spitz, D. & Lemke, E. A. (2016). Debugging Eukaryotic Genetic Code Expansion for Site-Specific Click-PAINT Super-Resolution Microscopy. *Angewandte Chemie International Edition*, *55*(52), 16172–16176. https://doi.org/10.1002/anie.201608284

Nour, A. M., Li, Y., Wolenski, J. & Modis, Y. (2013). Viral Membrane Fusion and Nucleocapsid Delivery into the Cytoplasm are Distinct Events in Some Flaviviruses. *PLoS Pathogens*, *9*(9), e1003585. https://doi.org/10.1371/journal.ppat.1003585

Olsson, M. H. M., Søndergaard, C. R., Rostkowski, M. & Jensen, J. H. (2011). PROPKA3: Consistent Treatment of Internal and Surface Residues in Empirical pKa Predictions. *Journal of Chemical Theory and Computation*, *7*(2), 525–537. https://doi.org/10.1021/ct100578z

Ou, W., Delisle, J., Konduru, K., Bradfute, S., Radoshitzky, S. R., Retterer, C., Kota, K., Bavari, S., Kuhn, J. H., Jahrling, P. B., Kaplan, G. & Wilson, C. A. (2010). Development and characterization of rabbit and mouse antibodies against ebolavirus envelope glycoproteins. *Journal of Virological Methods*, *174*(1–2), 99–109. https://doi.org/10.1016/j.jviromet.2011.04.003

bioRxiv preprint doi: https://doi.org/10.1101/2023.01.18.524651; this version posted January 20, 2023. The copyright holder for this preprint (which was not certified by peer review) is the author/funder. All rights reserved. No reuse allowed without permission.

780 Qin, F., Auerbach, A. & Sachs, F. (2000). A Direct Optimization Approach to Hidden Markov Modeling
781 for Single Channel Kinetics. *Biophysical Journal*, *79*(4), 1915–1927.
782 https://doi.org/10.1016/s0006-3495(00)76441-1

783 Rhoades, E., Ramlall, T. F., Webb, W. W. & Eliezer, D. (2006). Quantification of α-Synuclein Binding to
784 Lipid Vesicles Using Fluorescence Correlation Spectroscopy. *Biophysical Journal*, *90*(12), 4692–
785 4700. https://doi.org/10.1529/biophysj.105.079251

786 Saeed, M. F., Kolokoltsov, A. A., Albrecht, T. & Davey, R. A. (2010). Cellular Entry of Ebola Virus
787 Involves Uptake by a Macropinocytosis-Like Mechanism and Subsequent Trafficking through Early
788 and Late Endosomes. *PLoS Pathogens*, *6*(9), e1001110.
789 https://doi.org/10.1371/journal.ppat.1001110

790 Sakurai, Y., Kolokoltsov, A. A., Chen, C.-C., Tidwell, M. W., Bauta, W. E., Klugbauer, N., Grimm, C.,
791 Wahl-Schott, C., Biel, M. & Davey, R. A. (2015). Two-pore channels control Ebola virus host cell
792 entry and are drug targets for disease treatment. *Science*, *347*(6225), 995–998.
793 https://doi.org/10.1126/science.1258758

794 Salata, C., Calistri, A., Alvisi, G., Celestino, M., Parolin, C. & Palù, G. (2019). Ebola Virus Entry: From
795 Molecular Characterization to Drug Discovery. *Viruses*, *11*(3), 274.
796 https://doi.org/10.3390/v11030274

797 Schwarz, G. (1978). Estimating the Dimension of a Model. *The Annals of Statistics*, *6*(2).
798 https://doi.org/10.1214/aos/1176344136

799 Shi, L., Quick, M., Zhao, Y., Weinstein, H. & Javitch, J. A. (2008). The Mechanism of a
800 Neurotransmitter:Sodium Symporter—Inward Release of Na+ and Substrate Is Triggered by
801 Substrate in a Second Binding Site. *Molecular Cell*, *30*(6), 667–677.
802 https://doi.org/10.1016/j.molcel.2008.05.008

803 Simmons, J. A., D'Souza, R. S., Ruas, M., Galione, A., Casanova, J. E. & White, J. M. (2016). Ebolavirus
804 Glycoprotein Directs Fusion through NPC1 + Endolysosomes. *Journal of Virology*, *90*(1), 605–610.
805 https://doi.org/10.1128/jvi.01828-15

806 Singh, P., Mukherji, S., Basak, S., Hoffmann, M. & Das, D. K. (2022). Dynamic Ca2+ sensitivity
807 stimulates the evolved SARS-CoV-2 spike strain-mediated membrane fusion for enhanced entry.
808 *Cell Reports*, *39*(3), 110694. https://doi.org/10.1016/j.celrep.2022.110694

809 Søndergaard, C. R., Olsson, M. H. M., Rostkowski, M. & Jensen, J. H. (2011). Improved Treatment of
810 Ligands and Coupling Effects in Empirical Calculation and Rationalization of pKa Values. *Journal of*
811 *Chemical Theory and Computation*, *7*(7), 2284–2295. https://doi.org/10.1021/ct200133y

812 Spence, J. S., Krause, T. B., Mittler, E., Jangra, R. K. & Chandran, K. (2016). Direct Visualization of
813 Ebola Virus Fusion Triggering in the Endocytic Pathway. *MBio*, *7*(1), e01857-15.
814 https://doi.org/10.1128/mbio.01857-15

815 Straus, M. R., Tang, T., Lai, A. L., Flegel, A., Bidon, M., Freed, J. H., Daniel, S. & Whittaker, G. R.
816 (2020). Ca 2+ Ions Promote Fusion of Middle East Respiratory Syndrome Coronavirus with Host
817 Cells and Increase Infectivity. *Journal of Virology*, *94*(13). https://doi.org/10.1128/jvi.00426-20

bioRxiv preprint doi: https://doi.org/10.1101/2023.01.18.524651; this version posted January 20, 2023. The copyright holder for this preprint (which was not certified by peer review) is the author/funder. All rights reserved. No reuse allowed without permission.

818 Urade, R., Hayashi, Y. & Kito, M. (1988). Endosomes differ from plasma membranes in the
819 phospholipid molecular species composition. *Biochimica et Biophysica Acta (BBA) -*
820 *Biomembranes*, *946*(1), 151–163. https://doi.org/10.1016/0005-2736(88)90468-3

821 Whitt, M. A. (2010). Generation of VSV pseudotypes using recombinant ΔG-VSV for studies on virus
822 entry, identification of entry inhibitors, and immune responses to vaccines. *Journal of Virological*
823 *Methods*, *169*(2), 365–374. https://doi.org/10.1016/j.jviromet.2010.08.006

824 Zaitseva, E., Yang, S.-T., Melikov, K., Pourmal, S. & Chernomordik, L. V. (2010). Dengue Virus Ensures
825 Its Fusion in Late Endosomes Using Compartment-Specific Lipids. *PLoS Pathogens*, *6*(10),
826 e1001131. https://doi.org/10.1371/journal.ppat.1001131

827 Zhao, Y., Ren, J., Harlos, K., Jones, D. M., Zeltina, A., Bowden, T. A., Padilla-Parra, S., Fry, E. E. &
828 Stuart, D. I. (2016). Toremifene interacts with and destabilizes the Ebola virus glycoprotein.
829 *Nature*, *535*(7610), 169–172. https://doi.org/10.1038/nature18615

830

831

bioRxiv preprint doi: https://doi.org/10.1101/2023.01.18.524651; this version posted January 20, 2023. The copyright holder for this preprint (which was not certified by peer review) is the author/funder. All rights reserved. No reuse allowed without permission.

832 **Figures**

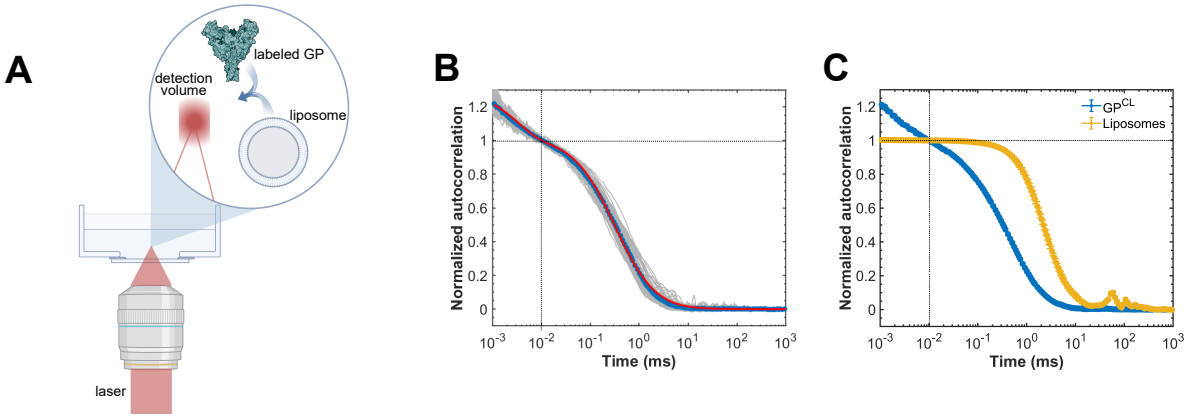

833 Figure 1

834 **Figure 1: FCS reports on GP-membrane interaction.** (**A**) Experimental setup of FCS assay for
835 quantifying GP-membrane interactions. A confocal spot is positioned in a dilute solution of Cy5-
836 labelled GP^{CL} with or without liposomes. Fluorescent particles are detected upon diffusion through
837 the confocal volume. (**B**) Autocorrelation data obtained from unbound Cy5-labelled GP^{CL}. The
838 autocorrelation of individual 5-sec fluorescence intensity traces was calculated (grey curves). The
839 average of 100 autocorrelation curves was calculated (blue) and fitted to a model for a single species
840 diffusing in 3 dimensions with a photophysical dynamics component (red). Accordingly, GP^{CL} has a
841 diffusion time of τ_D = 0.308 ± 0.007 ms. Photophysical dynamics were observed below 10^{-2} ms. (**C**)
842 Autocorrelation curves comparing diffusion times of GP^{CL} (blue) and liposomes (yellow). The diffusion
843 time of liposomes is 2.6 ± 0.2 ms, which is 8-fold longer than GP^{CL}, allowing for identification of
844 membrane-bound and unbound GP^{CL} in solution.

845

bioRxiv preprint doi: https://doi.org/10.1101/2023.01.18.524651; this version posted January 20, 2023. The copyright holder for this preprint (which was not certified by peer review) is the author/funder. All rights reserved. No reuse allowed without permission.

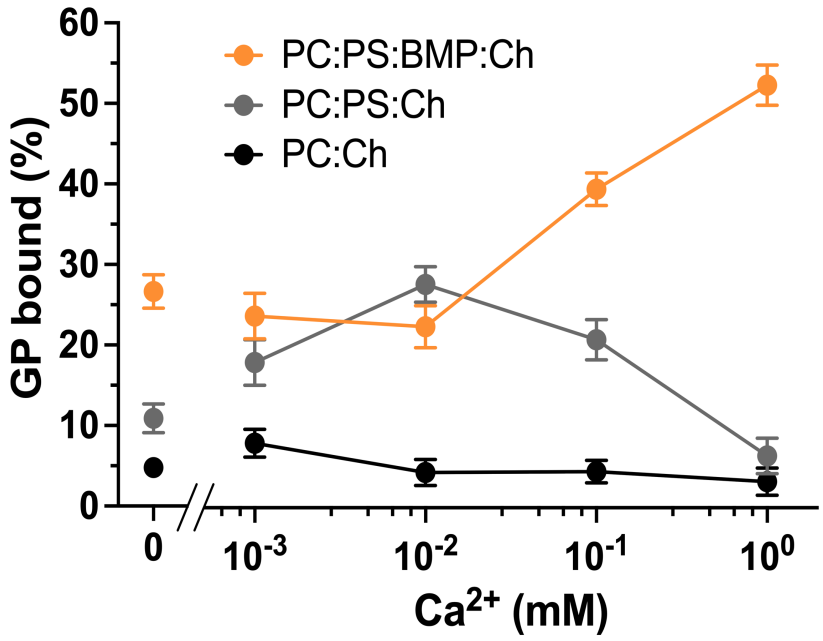

Figure 2

Figure 2: Anionic phospholipids and Ca^{2+} promote GP^{CL}-membrane interaction. The percentage of GP^{CL} bound to liposomes was determined using the FCS assay depicted in **Figure 1A**. Autocorrelation data were obtained from a solution of Cy5-labelled GP^{CL} and unlabelled liposomes and fit to a 3-dimensional diffusion for two species, membrane-bound and unbound GP^{CL} with diffusion times of 0.3 ms and 2.6 ms, respectively (Materials and Methods). Membrane binding to liposomes of varying lipid compositions was measured at pH 5.5 as a function of Ca^{2+} concentration: PC:Ch (black circles), PC:PS:Ch (grey circles) and PC:PS:BMP:Ch (orange circles). Data points reflect the mean ± standard error determined from three sets of measurements.

bioRxiv preprint doi: https://doi.org/10.1101/2023.01.18.524651; this version posted January 20, 2023. The copyright holder for this preprint (which was not certified by peer review) is the author/funder. All rights reserved. No reuse allowed without permission.

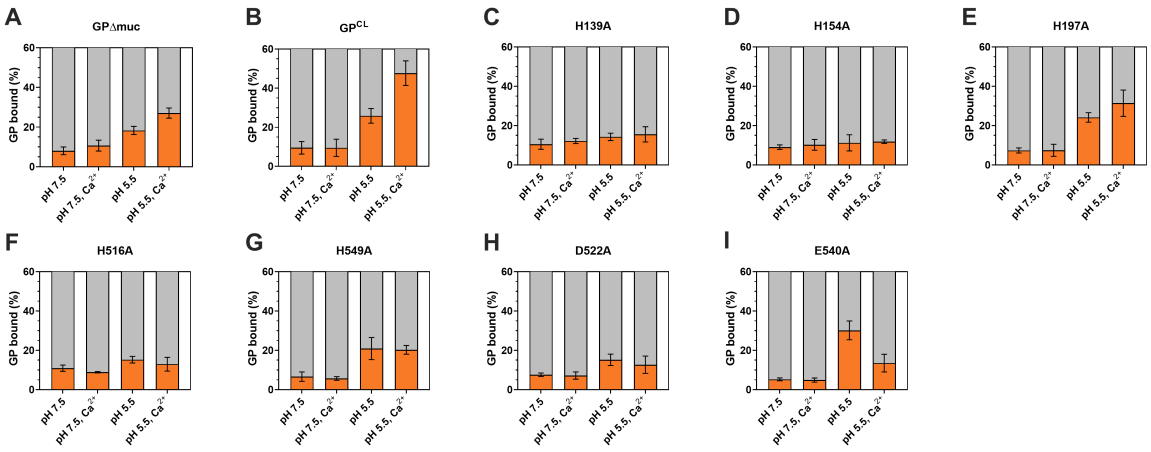

Figure 3

Figure 3: Conserved histidines and acidic residues mediate GP-membrane interaction. Membrane binding of (**A**) GPΔmuc, (**B**) GP^{CL} to PC:PS:BMP:Ch liposomes at neutral and acidic pH in the presence or absence of 1 mM Ca^{2+} is compared with the following mutants: (**C**) H139A, (**D**) H154A, (**E**) H197A, (**F**) H516A, (**G**) H549A, and (**H**) D522A, and (**I**) E540A, respectively. To ensure sensitivity to changes in the percentage of membrane binding of mutant GP^{CL}, a total lipid concentration of 500 µM was used such that a maximum of 50% wild-type GP^{CL} bound to liposomes at low pH in the presence of Ca^{2+}. The mean and standard error were calculated from three independent experiments.

bioRxiv preprint doi: https://doi.org/10.1101/2023.01.18.524651; this version posted January 20, 2023. The copyright holder for this preprint (which was not certified by peer review) is the author/funder. All rights reserved. No reuse allowed without permission.

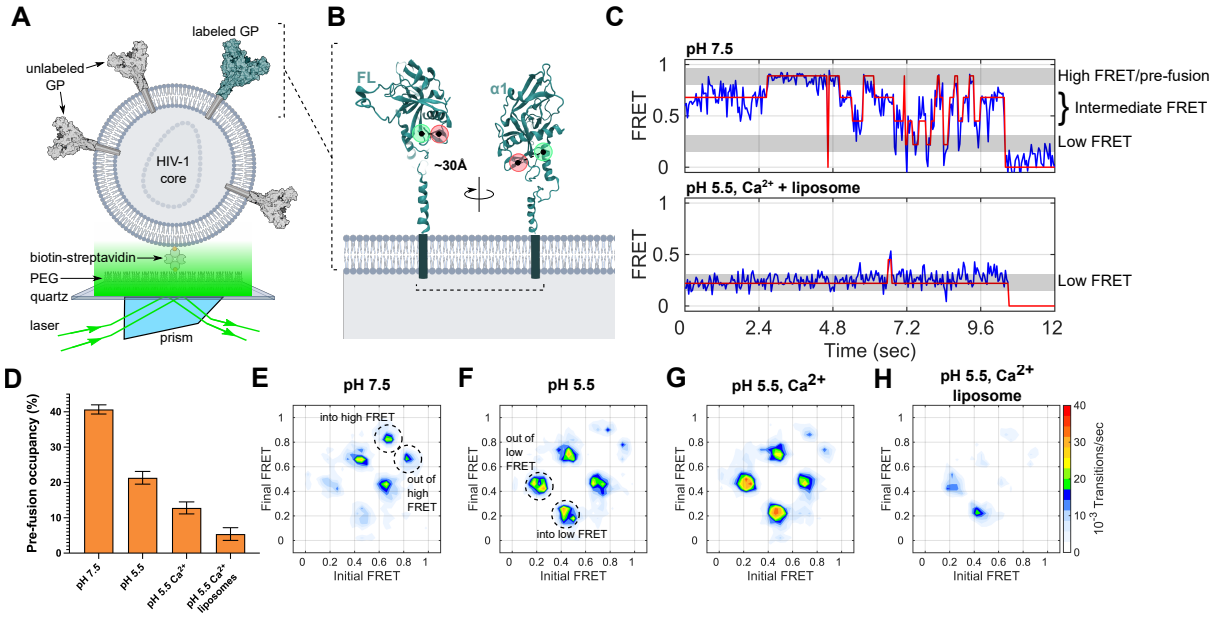

Figure 4

Figure 4: Acidic pH, Ca^{2+} and target membrane regulate GP conformational dynamics. (**A**) Experimental setup for smFRET imaging of pseudovirions labelled with the Cy3 and Cy5 FRET pair. Labelled pseudovirions were immobilized on a PEG-coated quartz microscope slide via a biotin-streptavidin covalent linkage and imaged using prism-based TIRF microscopy. (**B**) Fluorophore attachment positions (red and green circles; residues 501 and 610 in GP2) indicated on a GP protomer (PDB: 5JQ3). The indicated distance of 30 Å was previously determined through MD simulation of the fluorophore-labelled trimer (Das et al., 2020). (**C**) Representative FRET trajectories (blue) of GP^{CL} overlaid with idealization (red) determined through HMM analysis. The trajectory acquired at pH 7.5 (top) shows transitions between the pre-fusion conformation (0.92 FRET), two intermediate-FRET states (0.72 and 0.49), and a low-FRET state (0.24 FRET). In contrast, the FRET trajectory acquired in the presence of liposomes at pH 5.5 and 1 mM Ca^{2+} shows predominantly low FRET indicating a conformation stabilized by the presence of a target membrane. (**D**) Pre-fusion high-FRET state (0.92 FRET) occupancy of GP^{CL} determined under the indicated conditions through HMM analysis. The mean and standard error were calculated from three independent experiments. TDPs displaying the relative frequency of transitions of GP^{CL} at (**E**) pH 7.5, (**F**) pH 5.5, (**G**) pH 5.5 with 1 mM Ca^{2+}, and (**H**) after incubation with PC:PS:BMP:Ch liposomes for 20 min at 37°C, at pH 5.5 and 1 mM Ca^{2+}. Transitions into and out of high- and low-FRET states are depicted in (E) and (F), respectively.

bioRxiv preprint doi: https://doi.org/10.1101/2023.01.18.524651; this version posted January 20, 2023. The copyright holder for this preprint (which was not certified by peer review) is the author/funder. All rights reserved. No reuse allowed without permission.

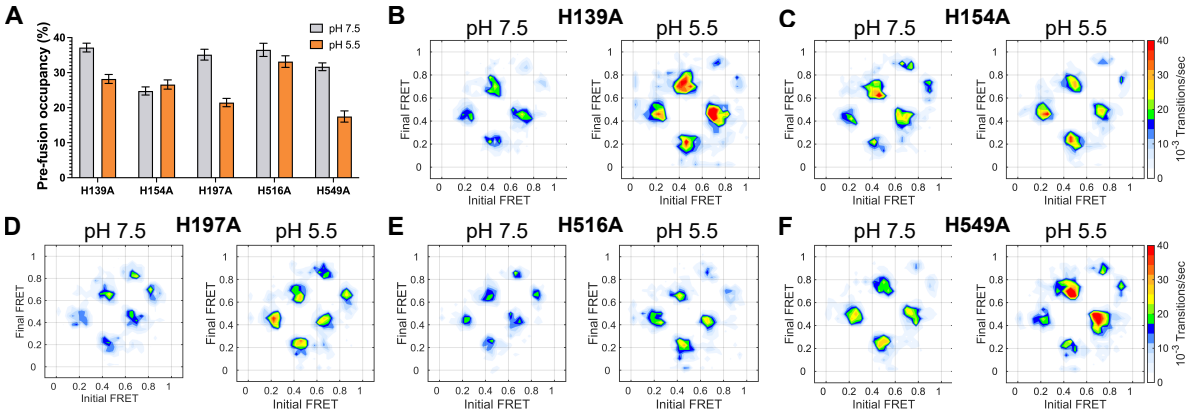

Figure 5

Figure 5: Conformational dynamics of GP histidine mutants. (**A**) Pre-fusion high-FRET state occupancy of GP mutants, determined at pH 7.5 (grey bars) and pH 5.5 (orange bars). The mean and standard error were calculated from three independent experiments. TDPs indicating the relative frequency of conformational transitions at pH 7.5 and pH 5.5, as indicated, for (**B**) H139A, (**C**) H154A, (**D**) H197A, (**E**) H516A, and (**F**) H549A.

bioRxiv preprint doi: https://doi.org/10.1101/2023.01.18.524651; this version posted January 20, 2023. The copyright holder for this preprint (which was not certified by peer review) is the author/funder. All rights reserved. No reuse allowed without permission.

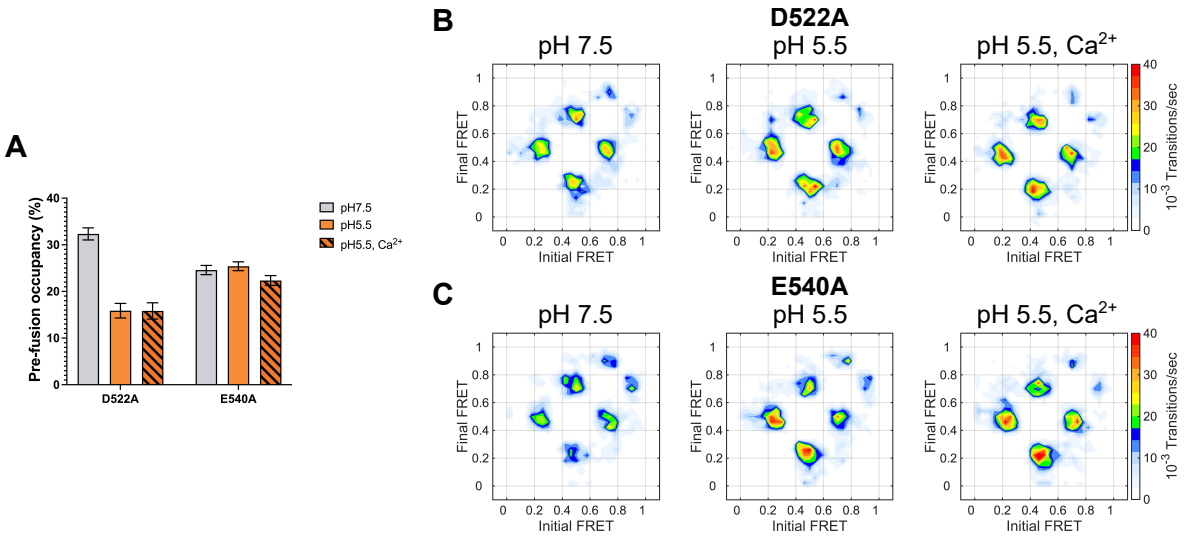

Figure 6

Figure 6: Conformational dynamics of GP with mutations in putative Ca^{2+}-coordinating residues. (**A**) Pre-fusion high-FRET state occupancy of GP mutants, determined at pH 7.5 (grey bars), pH 5.5 (orange bars), and pH 5.5 with 1 mM Ca^{2+} (orange striped bars). The mean and standard error were calculated from three independent experiments. TDPs indicating the relative frequency of conformational transitions determined under the indicated conditions for (**B**) D522A and (**C**) E540A.

bioRxiv preprint doi: https://doi.org/10.1101/2023.01.18.524651; this version posted January 20, 2023. The copyright holder for this preprint (which was not certified by peer review) is the author/funder. All rights reserved. No reuse allowed without permission.

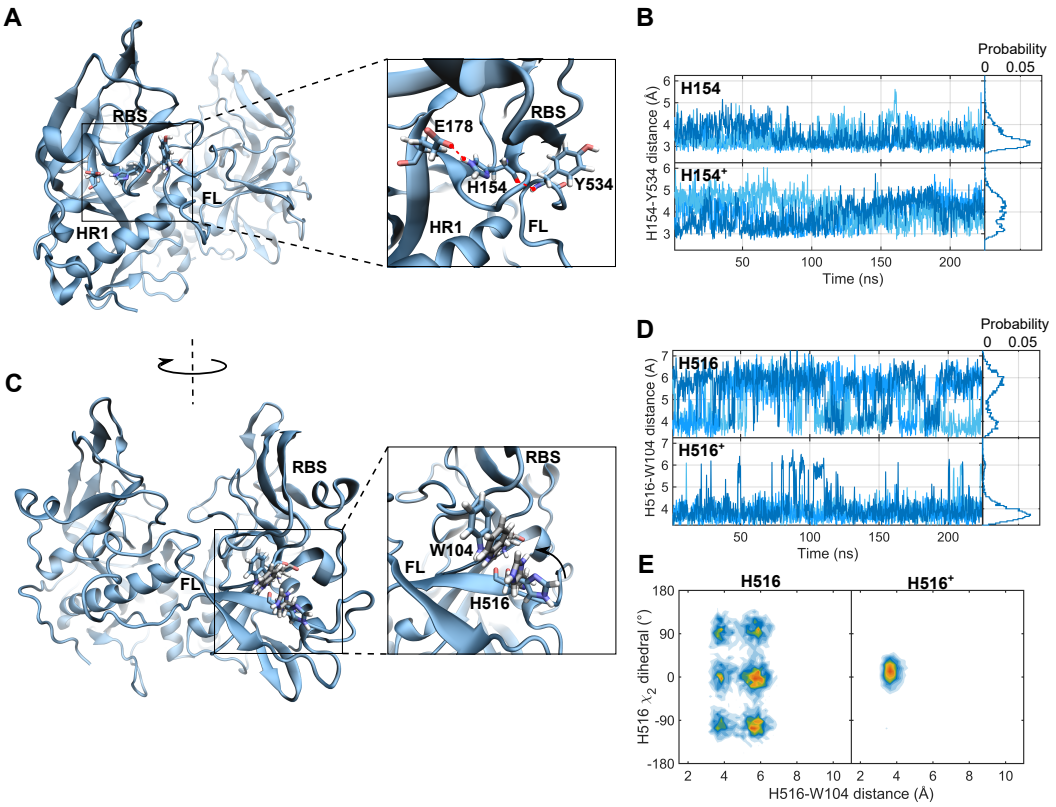

Figure 7

Figure 7: MD simulation provides molecular insights into pH-induced destabilisation of pre-fusion GP. (**A**) The simulation predicted electrostatic interactions between the side chains of H154 and E178, as well as between the backbones of H154 and Y534 in the fusion loop of the neighbouring protomer (red dotted lines). (**B**) The distances between the backbone N of H154 and the backbone carbonyl O of Y534 for each of the three protomers in the GP trimer (three shades of blue) determined from the simulation with (top) deprotonated histidines and (bottom) protonated histidines. Protonation of H154 increases the relative motion of H154 and Y534 as a result of stabilized H154-E178 interaction. (**C**) The simulation also predicts Pi-Pi stacking interaction between H516 in GP2 and W104 in GP1 with both (blue residues) deprotonated and (grey residues) protonated H516. (**D**) Distance trajectories indicating reduced H516-W104 distance under (top) deprotonated and (bottom) protonated conditions for the three protomers in the trimer (three shades of blue). Protonation of H516 (grey residues in (C)) stabilizes the interaction, drawing the two side chains into closer proximity. (**E**) Bivariate histogram of H516-W104 distances and H516 side-chain dihedral angles under (left) deprotonated and (right) protonated conditions. Fewer H516 conformations are available following protonation.

bioRxiv preprint doi: https://doi.org/10.1101/2023.01.18.524651; this version posted January 20, 2023. The copyright holder for this preprint (which was not certified by peer review) is the author/funder. All rights reserved. No reuse allowed without permission.

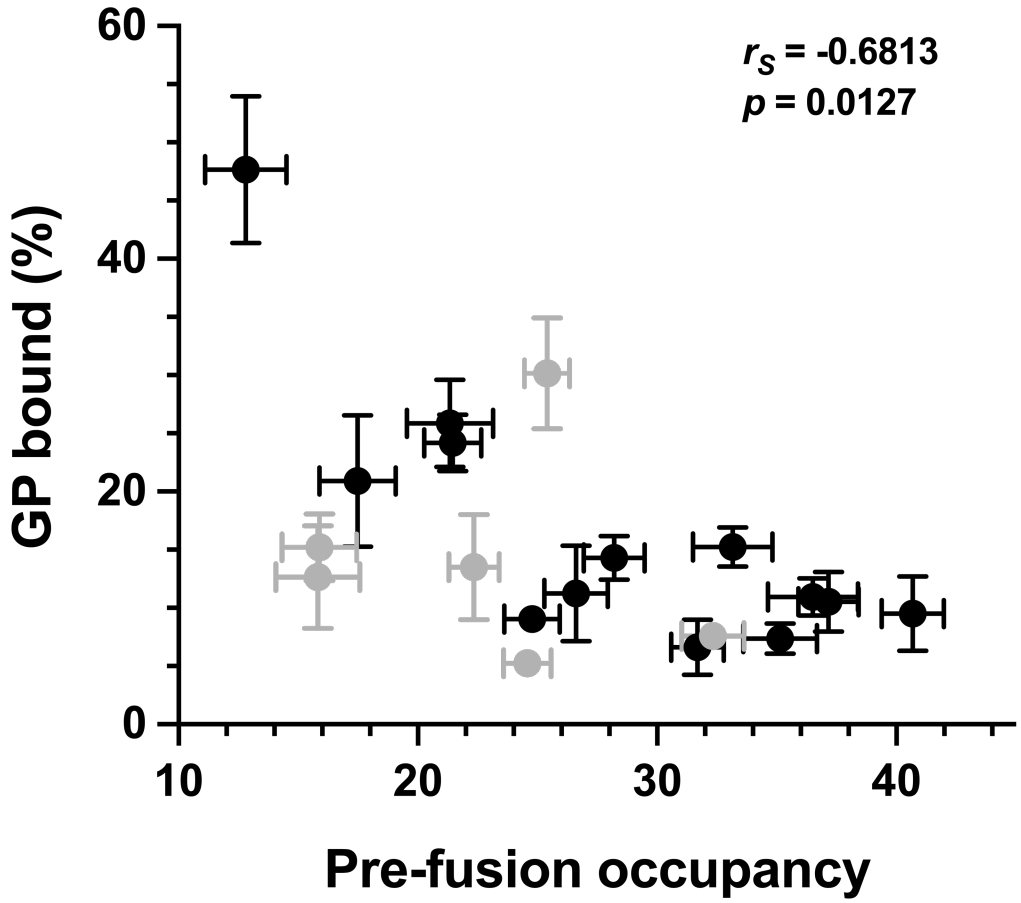

Figure 8

Figure 8: GP occupancy in the pre-fusion high-FRET conformation is inversely correlated with the extent of membrane binding. High-FRET state occupancy was determined through HMM analysis of smFRET trajectories. Membrane binding was determined by FCS. The non-parametric Spearman's correlation coefficient (r_S) and associated p-value are indicated. Data for D522A and E540A (grey points) does not correlate with membrane binding and were excluded from the analysis.